

THE EARLY CHEMICAL ENRICHMENT HISTORIES OF TWO SCULPTOR GROUP DWARF GALAXIES AS REVEALED BY RR LYRAE VARIABLES

SOUNG-CHUL YANG^{1, 2, +}, RACHEL WAGNER-KAISER³, ATA SARAJEDINI³, SANG CHUL KIM¹, AND JAEMANN KYEONG¹

¹Korea Astronomy and Space Science Institute (KASI), Daejeon, 305-348, South Korea

²The Observatories of the Carnegie Institution for Science, 813 Santa Barbara Street, Pasadena, CA 91101, U SA and

³Department of Astronomy, University of Florida, P.O. Box 112055, Gainesville, FL 32611

Accepted to The Astrophysical Journal

ABSTRACT

We present the results of our analysis of the RR Lyrae (RRL) variable stars detected in two transition-type dwarf galaxies (dTrans), ESO294-G010 and ESO410-G005 in the Sculptor group, which is known to be one of the closest neighboring galaxy groups to our Local Group. Using deep archival images from the Advanced Camera for Surveys (ACS) onboard the Hubble Space Telescope (HST), we have identified a sample of RR Lyrae candidates in both dTrans galaxies [219 RRab (RR0) and 13 RRC (RR1) variables in ESO294-G010; 225 RRab and 44 RRC stars in ESO410-G005]. The metallicities of the individual RRab stars are calculated via the period-amplitude-[Fe/H] relation derived by Alcock et al. This yields mean metallicities of $\langle [Fe/H] \rangle_{ESO294} = -1.77 \pm 0.03$ and $\langle [Fe/H] \rangle_{ESO410} = -1.64 \pm 0.03$. The RRL metallicity distribution functions (MDFs) are investigated further via simple chemical evolution models; these reveal the relics of the early chemical enrichment processes for these two dTrans galaxies. In the case of both galaxies, the shapes of the RRL MDFs are well-described by pre-enrichment models. This suggests two possible channels for the early chemical evolution for these Sculptor group dTrans galaxies: 1) The ancient stellar populations of our target dwarf galaxies might have formed from the star forming gas which was already enriched through “prompt initial enrichment” or an “initial nucleosynthetic spike” from the very first massive stars, or 2) this pre-enrichment state might have been achieved by the end products from more evolved systems of their nearest neighbor, NGC 55. We also study the environmental effects of the formation and evolution of our target dTrans galaxies by comparing their properties with those of 79 volume limited ($D_{\odot} < 2$ Mpc) dwarf galaxy samples in terms of the luminosity-metallicity relation and the H I gas content. The presence of these RRL stars strongly supports the idea that although the Sculptor Group galaxies have a considerably different environment from the Local Group (e.g. no giant host galaxies, loosely bound and very low local density), they share a common epoch of early star formation with the dwarf satellite galaxies in the Local Group.

Subject headings: galaxies: formation – galaxies: evolution – (galaxies:) Local Group – stars: variables: RR Lyrae

1. INTRODUCTION

The chemical evolution of galaxies during their earliest stages provides important insights for the initial physical and environmental conditions of the galaxy formation process. The star formation history (SFH) of galaxies is one of the important factors determining the path of their chemical evolution because the number of stars formed (i.e. the star formation rate) with a given initial mass function (IMF) controls the rate of chemical enrichment (Matteucci 2012). One key observable signature of the SFH of a galaxy is the metallicity distribution function (MDF) of its stars. Thus, we can test possible scenarios for the early epochs of galaxy formation by comparing the observed MDF of the oldest stellar population in the galaxy with several analytical models of chemical evolution.

In this context, the Sculptor group dwarf galaxies provide an excellent test bed for investigating the early chemical evolution of dwarf satellite galaxies formed in low density environments (i.e. outskirts of dense galaxy clusters, Local Group-like group environment, or field-

like environment; see Section 4.4 of the present study). The Sculptor group, also known as the Sculptor filament, is one of the closest groups of galaxies to our Local Group (i.e. distance to the group center, $d_{gc} \sim 3.9$ Mpc; Karachentsev et al. 2003). Five bright late-type galaxies (NGC 55, 247, 253, 300, and 7793) and at least 16 dwarf satellites form a very loosely bound, field-like system stretched along the line of sight over ~ 5 Mpc. Our target galaxies, ESO294-G010 and ESO410-G005, are Phoenix-like transition-type dwarf galaxies (dTrans) that morphologically resemble the gas-poor dwarf spheroidal galaxies (dSphs) but contain detectable amounts of neutral hydrogen (H I) gas (i.e. $\sim 10^5 M_{\odot}$; Bouchard et al. 2005; Jerjen, H., Freeman, K. C., & Bingeli, B. 1998), and show signs of recent star formation activity. Most recently, from their detailed analysis of the color-magnitude diagrams obtained using deep HST/ACS imaging for the five Sculptor group dwarf galaxies, Lianou et al. (2013; hereafter L13) found population gradients in ESO294-G010 and ESO410-G005 in the sense that young blue main sequence stars (age < 100 Myr) and intermediate age asymptotic giant branch stars (age ~ 1 -2 Gyr) are more centrally concentrated, while old horizontal branch stars (age > 10 Gyr) tend to

sczoo@kasi.re.kr

⁺ KASI-Carnegie Fellow

be more spatially extended.

The high quality of those HST/ACS images also allowed the first detection of a significant population of RR Lyrae variable star candidates beyond the Local Group. Da Costa et al. (2010) were able to discover numerous RR Lyrae candidates in both dTrans galaxies using a template light curve technique (Layden 1998). The presence of the RR Lyrae stars in ESO294-G010 and ESO410-G005 directly confirms the existence of ancient stellar populations with ages > 10 Gyr and indicates that the Sculptor group dwarf galaxies share a common epoch of the earliest star formation with our Local Group galaxies even though these two groups of galaxies have quite different local density environments.

In addition to being a direct probe of ancient stellar populations, RR Lyrae stars provide a variety of utilities to investigate a number of important astrophysical applications; these stars are well-known reliable population II distance indicators. There is a correlation between the metallicities and the pulsation properties (i.e. periods and amplitudes) of the fundamental mode RR Lyrae stars (RR0 or RRab). Using this relation (Alcock et al. 2000; Sarajedini et al. 2006), we can calculate the metallicities of individual RRab stars, and thus construct the MDF for a purely old stellar population. Lastly, the intrinsic colors of RRab stars at their faintest luminosity are largely independent of their other physical properties [$(V - I)_{0,min} = 0.58 \pm 0.02$; Guldenschuh et al. 2005], therefore using their observed colors at minimum light we can also estimate the line-of-sight reddening.

The main goal of the present study is to examine the MDFs of legitimate RR Lyrae stars in the two Sculptor group dTrans galaxies, ESO294-G010 and ESO410-G005, in order to investigate the early chemical evolution of these systems, especially in light of the low density environments in which they reside. This paper is organized as follows. Section 2 provides a description of the data set and photometry process. In section 3 we report the results of our analysis including the general trends in the color-magnitude diagrams (CMDs) of the galaxies (Sec 3.1), the details of our RR Lyrae detection method and the pulsation properties of the RR Lyrae candidates (sec 3.2), the calculation of the metallicities of individual RR Lyraes (sec 3.3), and the distance measurements (sec 3.4). In section 4 based on our estimates in the previous sections, we present our in depth discussion on the star formation histories, early chemical evolutions, the luminosity-metallicity relations of the our target dTrans, and the environmental effects on the evolution of the near field dwarf galaxies. Finally in section 5 we present a summary of our results.

2. OBSERVATIONS AND DATA REDUCTION

The science images of ESO294-G010 and ESO410-G005 used in this study were taken with the Advanced Camera for Surveys Wide Field Channel (ACS/WFC) on board *Hubble Space Telescope* (HST) as a part of GO-10503 (PI: Da Costa). The observing log for the retrieved archival images is shown in Table 1. The detailed observing strategy has been provided by Da Costa et al. (2010). To briefly describe the observations, the central regions of each galaxy were placed on one of WFC chips

so that the imaging covers almost the entire visual extent of the targets. ESO294-G010 was imaged 12 times in the F606W and 24 times in the F814W filter with an exposure time of 1160s during the observing baseline of ~ 1.86 days. The same number of exposures were obtained for the observations of ESO410-G005 with an exposure time of 1120s over the observing baseline of 4.55 days. In this way the observations provide a good quality time-series photometry that allows us to detect genuine RR Lyrae variable candidates in each galaxy.

We photometered the point sources in the cosmic-ray cleaned *crj* images with the ACS module of DOLPHOT package (Dolphin 2000) by following the standard procedures for DOLPHOT. These *crj* images are calibrated FITS images that were produced through the ACS Calibration (CALACS) pipeline, which performs basic image reduction and data calibration including cosmic ray rejection. Pre-constructed point spread functions (PSFs) for each ACS passband were used to expedite the PSF photometry. Once bad pixels were removed, each ACS/WFC image which contains both chips was split into two separate image files with single-chip format. Then, all of the individual images were aligned and photometered simultaneously. Aperture corrections were calculated for each image with the default settings of DOLPHOT. The instrumental magnitudes were transformed to the native ACS/WFC VEGAmag system as well as the ground-based Johnson-Cousins VI system using the calibration equations of Sirianni et al. (2005) implemented in DOLPHOT. The resultant magnitudes were corrected for the loss of charge transfer efficiency (CTE) as described in ACS ISR 2003-09. We performed photometric completeness tests using the artificial star feature (“acsfakelist”) in DOLPHOT. This experiment allows us to gauge the degree of photometric completeness, as well as photometric errors.

The final set of standard VI photometry was extracted from the resultant file by selecting only those stars with “object type” equal to 1 (i.e. a good star). These stars also meet the additional selection criteria set by the several photometric quality parameters: $S/N > 10$, $-0.5 < Sharpness_{F606W} < +0.5$, and $-1 < Crowding_{F606W} < +1$. The sharpness approaches zero for a star with a nearly perfect stellar profile, while for a source that is too sharp (i.e. a cosmic ray) this value becomes positive. A negative value indicates a source that is extended or too broad (i.e. a blend, cluster or galaxy). According to the test done by Dolphin et al. (2004), good stars in an uncrowded field should have sharpness values between -0.3 or $+0.3$. The crowding parameter is defined in magnitude units. For an isolated star, the value is zero. For stars in a highly crowded field, this value becomes larger than unity (positive or negative).

3. RESULTS

3.1. Color-Magnitude Diagrams

Color-magnitude diagrams (CMDs) of ESO294-G010 and ESO410-G005 in the standard VI system are presented in Figures 1 and 2. Our artificial star tests show that the point sources in both galaxies are well photometered to ~ 2 magnitude below the horizontal branch (HB) level with better than $\sim 50\%$ photometric completeness (see the right panels of Fig 1 & Fig 2). At the level of the

TABLE 1
OBSERVATION LOG.

Object	RA (J2000)	Dec. (J2000)	Filters	Data Set	HJD Range (+2 453 000)
ESO294-G010	00 26 33.40	-41 51 19.0	F606W	12x1160s	j9bd0701*,j9bd0801*,j9bd1202*
			F814W	24x1160s	j9bd0702*,j9bd0802*,j9bd0901*-j9bd1201*
ESO410-G005	00 15 31.40	-32 10 47.0	F606W	12x1120s	j9bd1301*,j9bd1401*,j9bd1802*
			F814W	24x1120s	j9bd1302*,j9bd1402*,j9bd1501*-j9bd1801*

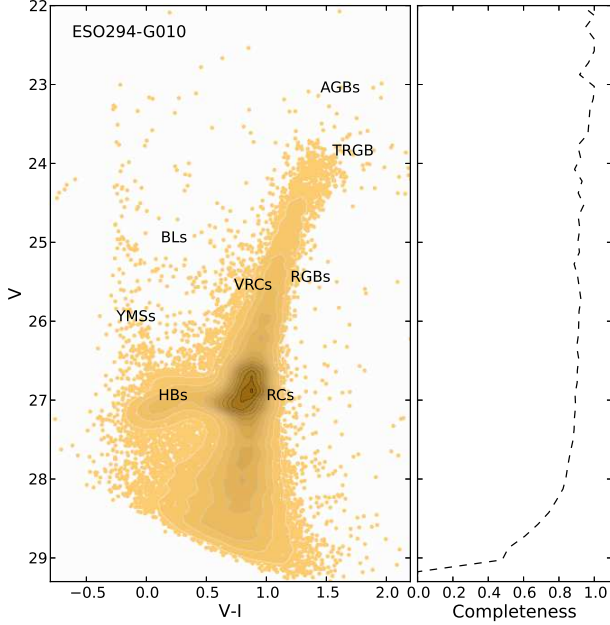
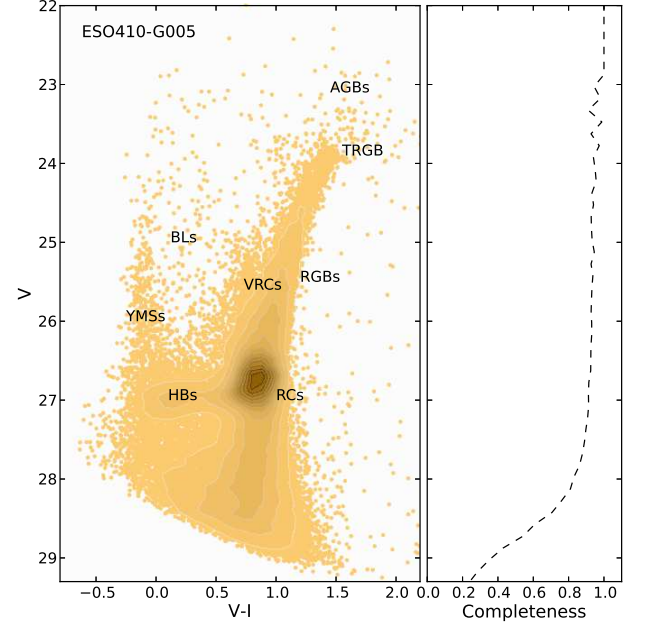

 FIG. 1.— The VI color-magnitude diagram of ESO294-G010 (see section 3.1. for the detail explanations of each label). The right-hand panel illustrates the photometric completeness indicating that our photometry is as complete as $\sim 88\%$ at the level of horizontal branch magnitude.


FIG. 2.— The VI color-magnitude diagram of ESO410-G005 (see section 3.1. for the detail explanations of each label). The photometric completeness is comparable to that for ESO294-G010.

HB magnitude the photometric completeness reaches $\sim 88\%$. Therefore we assume that photometric incompleteness does not significantly affect our analysis of the RR Lyrae variable stars.

According to the morphological type T (de Vaucouleurs et al. 1991; Karachentsev et al. 2004), and the classifications for dwarf galaxies (Mateo 1998), both ESO294-G010 ($T=-3$) and ESO410-G005 ($T=-1$) satisfy the criteria of transition-type dwarf galaxies (dTrans) that exhibit reduced recent star formation but relatively high gas fractions. The tidal indices (Θ ; Karachentsev et al. 2004, 2013; also see Section 4.4. of the present study) of these two dTrans systems indicate that they are gravitationally bound to their nearest neighbor, NGC 55 which is a nearly edge-on barred irregular galaxy.

In general, given that these two dTrans galaxies have comparable mass and size, the CMDs of ESO294-G010 and ESO410-G005 show a close resemblance to each other. Both of the two dTrans feature diverse stellar constituents with wide ranges of age and metallicity: young blue main-sequence stars (YMSs), relatively weak but recognizable intermediate mass He core-burning blue

loop stars (BLs), a handful of vertical extension red clump stars (VRCs) and asymptotic giant branch stars (AGBs) both of which represent intermediate-age (1 – 10 Gyr) populations, dominant first ascent red giant branch stars (RGBs), tightly gathered red clump stars (RCs), and distinctively stretched horizontal branch stars (HBs) that strongly signal an ancient stellar population (age > 10 Gyr). Detailed descriptions of each characteristic stellar constituent in these two galaxies can be found in the recent work of L13.

3.2. RR Lyrae Stars

3.2.1. Detection and Characterization

We employed the technique of Yang et al. (2010; Y10 hereafter) and Yang & Sarajedini (2012; YS12 hereafter) to identify and characterize RR Lyrae stars in ESO294-G010 and ESO410-G005. In summary, we start by searching all possible variable star candidates at the level of the HB brightness ($26.5 < V < 27.6$). The variability of each star within the given range of V magnitude was evaluated by the reduced χ^2_{VI} defined by the following formula:

$$\chi_{VI}^2 = \frac{1}{N_V + N_I} \times \left[\sum_{i=1}^{N_V} \frac{(V_i - \bar{V})^2}{\sigma_i^2} + \sum_{i=1}^{N_I} \frac{(I_i - \bar{I})^2}{\sigma_i^2} \right], (1)$$

Any data points located more than $\pm 3\sigma$ from the mean magnitude were excluded from the calculation of χ_{VI}^2 . Only those stars with χ_{VI}^2 values greater than 3.0 were considered as potential variable candidates [i.e. typical non-variable stars at the HB level ($V(\text{HB}) \sim 27$) have χ_{VI}^2 values less than 3.0]. The VI time series photometry of the variable star candidates that satisfy our variability criterion was analyzed with our template light curve fitting routine, RRFIT, which fits both V and I band data simultaneously yields the best fitting light curve parameters such as period, amplitude, epoch at maximum light, and mean magnitudes (see YS12 for more details). Each output best-fit light curve was carefully examined by eye. Then in the VI CMDs, we checked the mean color and magnitude of those RR Lyrae candidates that passed our eye-inspection to make sure they are located in the expected region of the HB. Finally, in order to further ensure that our sample contains genuine RR Lyrae variables, we applied marginal V-I color ranges using the blue and red edges of the empirical instability strip for RR Lyrae variables from Mackey & Gilmore (2003) to which we added a 3σ rms error (i.e. $\sigma_{VI} = \pm 0.04$ mag) in the (V-I) colors at the level of the HBs. Figure 3 illustrates zoomed-in CMDs with the RR Lyrae candidates identified from our analysis. Both CMDs show that the bulk of genuine RRL candidates are well selected within the adopted V-I color ranges for each target galaxy.

After applying the above procedures, we have identified and characterized 232 RR Lyrae stars (219 RRab and 13 RRC) in ESO294-G010 and 269 RR Lyraes (225 RRab and 44 RRC) in ESO410-G005. Now we go back to the reference images to examine the individual RR Lyraes to see how many blended objects were included among the selected RR Lyrae samples. Our examination reveals that there are 73 blended objects (68 RRab + 5 RRC) among the 232 RRL samples in ESO294-G010, while we found 92 blended objects (73 RRab + 19 RRC) among the 269 RRL candidates in ESO410-G050. We further examine the pulsation properties (see Fig 9. Period-amplitude diagrams in section 3.2.3) of these objects to investigate whether the blending causes any systematic bias in the mean pulsation properties of our RR Lyrae samples. We find no indication of significant systematic biases in the period-amplitude space due to the blending; instead, we see that the blended objects follow the mean period-amplitude trend just like the other well-isolated RR Lyrae stars. Therefore we assume that our analyses in this study are not negatively affected by the effects of stellar blending. Figures 4–5 illustrate a sample of the best-fitting light curves for the RR Lyrae candidates. The basic properties of each of these RR Lyrae candidates are summarized in Tables 2–3.

We also attempted to search for other types of variable stars in both dTrans by expanding our search ranges in the color-magnitude ($24.0 < V < 26.7$; $-0.5 < V - I < 0.95$) and period ($0.4 < P < 3$ days) spaces. Then we apply the same method as we did for the RR Lyrae survey. We have uncovered a significant number of lu-

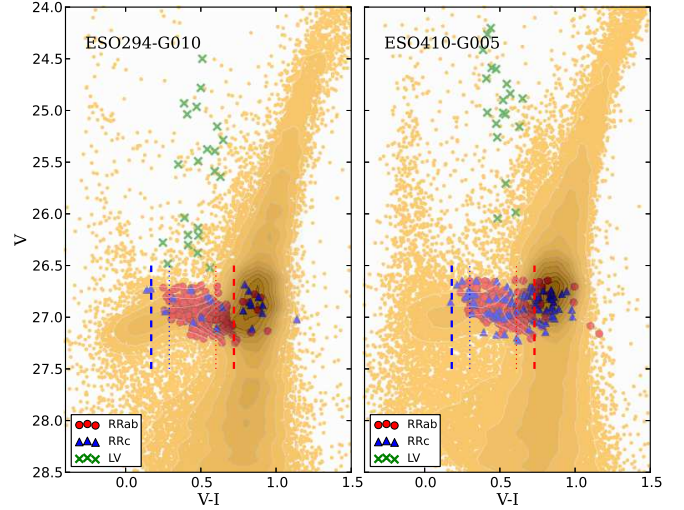


FIG. 3.— The zoomed-in VI color-magnitude diagrams with RR Lyrae candidates shown. The dotted lines illustrate the blue and red edges of the empirical instability strip (Mackey & Gilmore 2003) for each galaxy, while the dashed lines which were extended to both blue and red sides of the empirical instability strip by $3\sigma_{VI}$ indicate the V-I color range for our selection of the RR Lyrae candidates. Doing so we increase genuine RR Lyrae samples in each dTrans as many as possible; The green crosses indicate the luminous variable (LV) candidates. These stars probably include Anomalous Cepheids, Pop II Cepheids, and short-period Classical Cepheids.

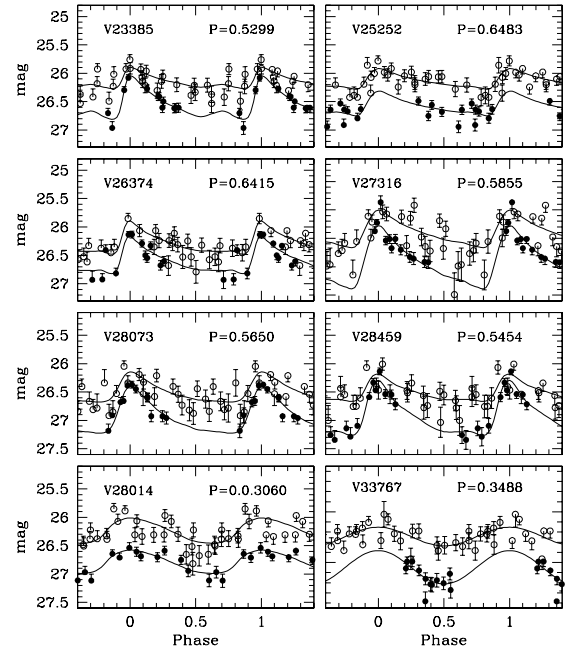


FIG. 4.— A sample of the best-fitting light curves for the RR Lyrae candidates in ESO294-G010. The solid dots represent V-band data, while I-band data are marked by open circles.

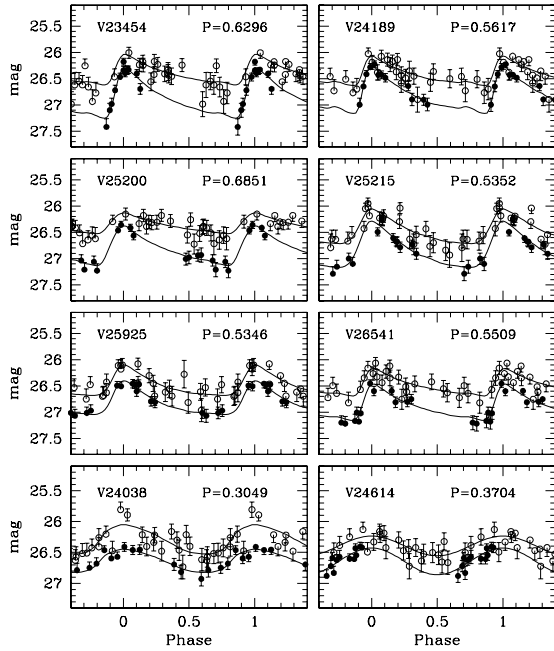
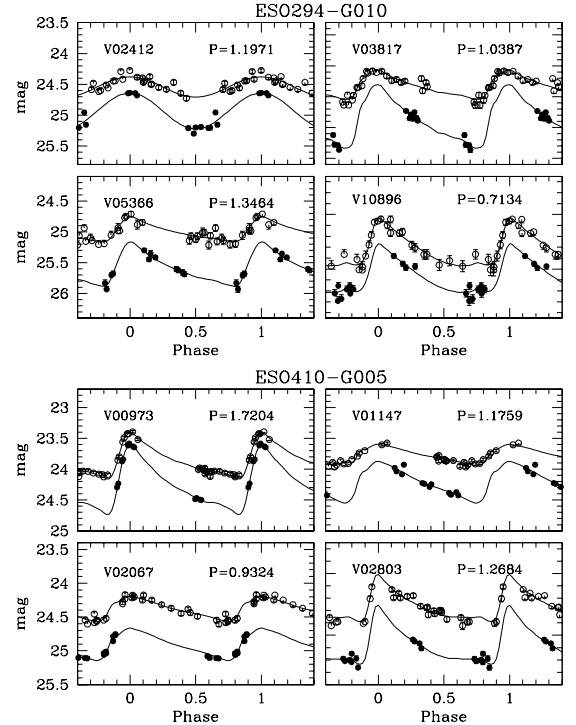


FIG. 5.— Same as Figure 4, but for ESO410-G005.

minous variable (LV) candidates in both dTrans (22 in ESO294-G010; 19 in ESO410-G005). Their photometric and pulsation properties are summarized in Table 4. Figure 6 illustrates some examples of the best-fitting light curves for the LV candidates in the two dTrans. These stars are brighter than the RRL group by 0.5 ~ 3.0 mag (see Fig 3). Their color-magnitude positions and period-amplitude properties appear to be consistent with those of typical Anomalous Cepheids, Pop II Cepheids, and short-period Classical Cepheids (Gallart et al. 2004; Pritzl et al. 2005; Bernard et al. 2009). We find that these LVs are more concentrated in the inner fields and their spatial distributions seem to be aligned with the major axis of the ellipsoid of each dTran, which might indicate that these stars belong to the young or intermediate-age populations of the dTrans (see the bottom panels of Fig 12).

3.2.2. Synthetic Light Curve Simulation

The derived pulsation parameters of RR Lyrae variables are often subject to spurious periods (or aliases) that are mainly caused by the effects of undersampling. In order to estimate the degree of any aliases in our period-searching analysis, we have performed extensive simulations and statistical tests (Y10; YS12; Sarajedini et al. 2012). Input periods and amplitudes were randomly generated within an appropriate range of ab-type and c-type RR Lyraes. We then produced ~1000 synthetic RR Lyrae light curves with these input periods and amplitudes by applying the observing windows - such as observing baseline, number of epochs, cadence, and photometric errors - that were extracted from the time series photometry of a well measured RR Lyrae candidate. Finally these synthetic VI time series photometry

FIG. 6.— A sample of the best-fitting light curves for the luminous variable candidates in our target galaxies. The *solid dots* represent V-band data, while I-band data are marked by *open circles*.

sets were analyzed by the RRFIT routine to check how well the output periods and amplitudes recover the input values. The comparison between the input and output solutions is presented in Figures 7–8 where we plot the distributions of the input and output periods (ΔP), and the difference between these two values as a function of input period.

The next step involved the following statistical test. From the artificial RR Lyrae lists, we randomly sample artificial RR Lyrae stars with the same number as the observationally detected RR Lyraes in each galaxy [ESO294-G010 : 219 (RRab) and 13 (RRc); ESO410-G005 : 225 (RRab) and 44 (RRc)] to examine their ΔP distribution. The $1\text{-}\sigma$ error (σ_P) of this ΔP distribution from the best-fit Gaussian can be considered as a good estimate of the standard error in the individual periods derived by our period-searching analysis. In order to improve the statistical robustness of the σ_P value, this random sampling was iterated 10,000 times. We then consider the average spread ($\langle \sigma_P \rangle$) of these 10,000 samples as a realistic error for our period measurements. The same approach was applied to estimate errors in the V-band amplitude.

We summarize here the main findings of our simulations.

1. For the RRab stars in ESO294-G010, ~ 80% of the input periods were well recovered within ± 0.05 day, while this recovery fraction was significantly reduced to ~ 25% for the RRc stars. In the case of ESO410-G005, this value becomes ~ 70% and 30% for the RRab and RRc respectively.

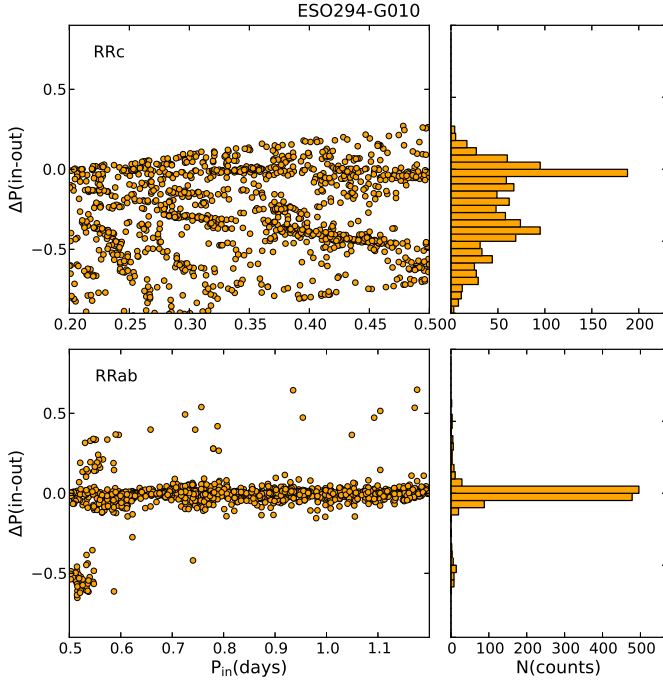


FIG. 7.— The results of our synthetic light curve simulations for ESO294-G010. Left panels illustrate the difference ($\Delta P = P_{in} - P_{out}$) between the input and output period as a function of the input period for two different pulsation modes. Right panels show the ΔP distributions. Our simulations reveal that type-c RR Lyrae stars are significantly influenced by aliasing while type-ab RR Lyrae stars are almost free from the effects of aliasing.

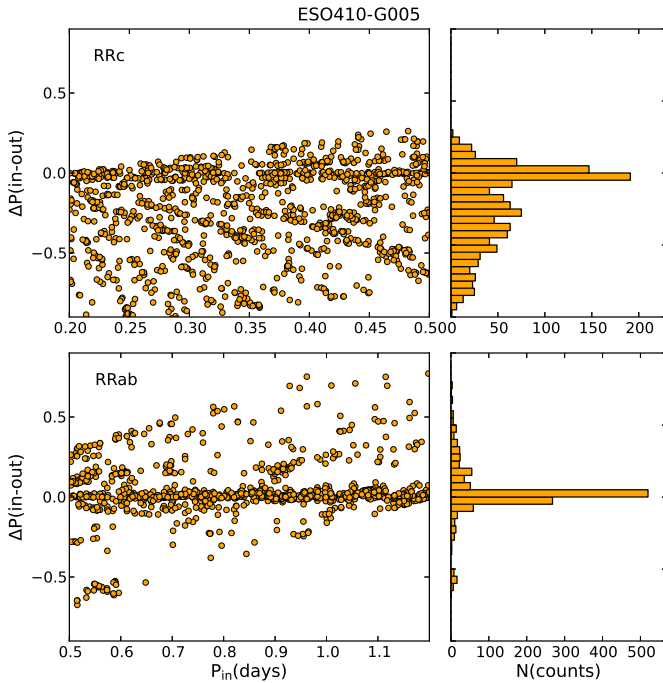


FIG. 8.— Same as Figure 7, but for ESO410-G005. Similar to the case of ESO294-G010, type-c RR Lyrae stars in ESO410-G005 are more severely affected by aliasing as compared with type-ab RR Lyrae stars.

2. The standard errors (σ_P/\sqrt{N}) of the individual RR Lyrae periods in our analysis are $\sigma(P_c) = \pm 0.0214$ and $\sigma(P_{ab}) = \pm 0.0006$ days for the RR Lyrae candidates found in ESO294-G010. For the ESO410-G005 RR Lyrae candidates, we find $\sigma(P_c) = \pm 0.0061$ and $\sigma(P_{ab}) = \pm 0.0008$ days. The errors in the V band amplitudes are $\sigma(Amp(V)_c) = 0.0214$ mag and $\sigma(Amp(V)_{ab}) = 0.0016$ mag for the ESO294-G010 RR Lyraes, while these values become $\sigma(Amp(V)_c) = 0.0013$ mag and $\sigma(Amp(V)_{ab}) = 0.0018$ mag for the ESO410-G005 RR Lyraes.
3. We found no significant biases in our determination of the mean periods and amplitudes for the R Rab stars. However, it is evident for both galaxies that RRc stars are subject to more significant aliasing as compared to R Rab stars. In addition there exists a systematic trend in the sense that the output periods of RRc stars tend to be longer than the input periods. Thus we conclude that the aliasing in the periods of RRc stars significantly hinders the accurate determination of the pulsation periods of these stars, and it is not possible in this study to utilize their pulsation properties to study other aspects of RR Lyrae stars.

3.2.3. Period-Amplitude Diagrams

It is well known that the period-amplitude (P-A) relations (i.e. Bailey diagram) of RR Lyrae stars in the Milky Way Galaxy (both in the Galactic Globular Clusters and the field Galactic Halo) exhibit the so called the Oosterhoff dichotomy: Oosterhoff type I (Oo I) systems tend to have intermediate metallicities and a mean pulsation period of ~ 0.55 days in the fundamental mode with a low RRc frequency ($N_c = n_c/n_{abc} = 0.2$), while Oosterhoff type II (Oo II) systems are generally metal-poor and have mean pulsation periods of ~ 0.65 days with a higher fraction of RRc stars ($N_c = 0.45$; Castellani & Quarta 1987). Thus the Bailey diagram can serve as a useful diagnostic tool for investigating the basic pulsation properties of the RR Lyrae populations.

In Figure 9 we plot the P-A relations and period distributions of our RR Lyrae candidates found in ESO294-G010 and ESO410-G005. The loci of Oosterhoff type I and II for the Galactic Globular Cluster (GGC) systems [straight lines (Clement & Rowe 2000); quadratic relations (Cacciari et al. 2005, Zorotovic et al. 2010)] are also plotted for comparison. Solid symbols [red dots (R Rab); blue triangles (RRc)] indicate the well-isolated RR Lyraes stars not affected by crowding, while the blended objects (see section 3.2.1) are marked with open symbols. According to Figure 9, the blended stars are indistinguishable from the other well-isolated RR Lyrae variables. Thus, we find no significant systematic biases in the period-amplitude space due to stellar blending. We see that the bulk of the R Rab candidates in these two dTrans galaxies appear to be more tightly distributed around the locus of the Oosterhoff I type GGCs, while there are no significant population of Oosterhoff II RR Lyraes in both galaxies. The mean pulsation periods of the R Rab candidates are $\langle P \rangle_{ab, ESO294} = 0.5932 \pm 0.0003$ (error1) ± 0.0006 (error2) days and $\langle P \rangle_{ab, ESO410} = 0.5898 \pm 0.0003$ (error1) ± 0.0008 (error2) for ESO294-G010 and ESO410-G005 respectively. The quoted value

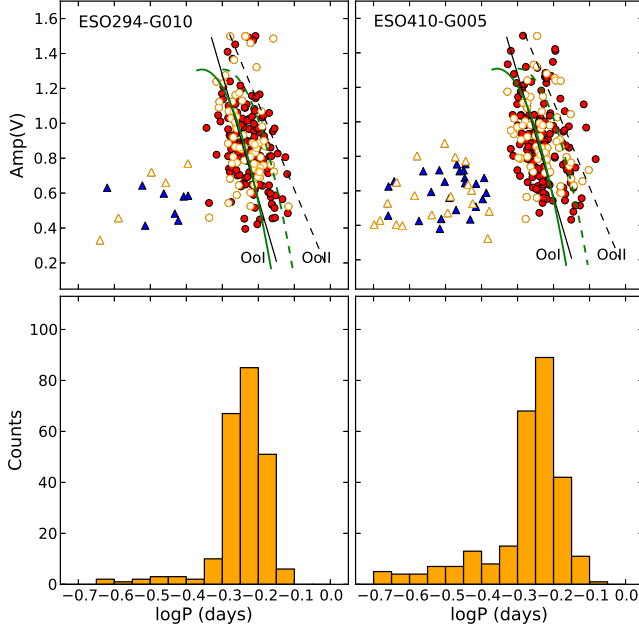


FIG. 9.— The Period-Amplitude (P-A) relations of the RR Lyrae candidates in ESO294-G010 and ESO410-G005 are plotted in the top panels. The bottom panels show the period distributions. The open symbols [circles (RRab or RR0); triangles (RRc or RR1)] represent the blend objects (see section 3.2.1), while the well-isolated RR Lyrae samples are marked with filled symbols [blue triangles and red dots]. Solid and dashed lines indicate the fiducials of Oosterhoff I and II systems [straight lines (Clement & Rowe 2000); quadratic relations (Cacciari et al. 2005, Zorotovic et al. 2010)]. The pulsation properties of the RR Lyrae candidates in these two Sculptor group dTrans appear to follow the typical trend for the RR Lyrae populations of Local Group dwarf satellite galaxies.

of “error1” represents the standard error of the mean and the “error2” value is the error derived from our synthetic light curve simulations.

3.3. Metallicity

RR Lyrae stars are very useful for tracing the early chemical enrichment histories of dwarf satellite galaxies. These pulsating variables represent a purely old stellar population (age > 10 Gyr) in a given galaxy. Hence, the advantage of using RR Lyrae for a robust measurement of the metal abundance of an ancient stellar population particularly stands out in the case of studying dTrans galaxies which exhibit recent star formation and diverse stellar populations with wide ranges of ages and metallicities.

The metal abundance of ab-type RR Lyrae can be calculated using the correlation between period, amplitude and $[Fe/H]$ given by Alcock et al. (2000) in the following form

$$[Fe/H] = -8.85[\log P_{ab} + 0.15 \text{Amp}(V)] - 2.60, (2)$$

where $\text{Amp}(V)$ indicates the V band amplitude, and $[Fe/H]$ is in the Zinn & West (1984) metallicity scale.

Figure 10 shows the metallicity distribution functions (MDFs; binned histograms and the best-fit gaussians) of the RRab stars found in the two dTrans galaxies of the present study. The MDF of the ESO294-G010 RRab

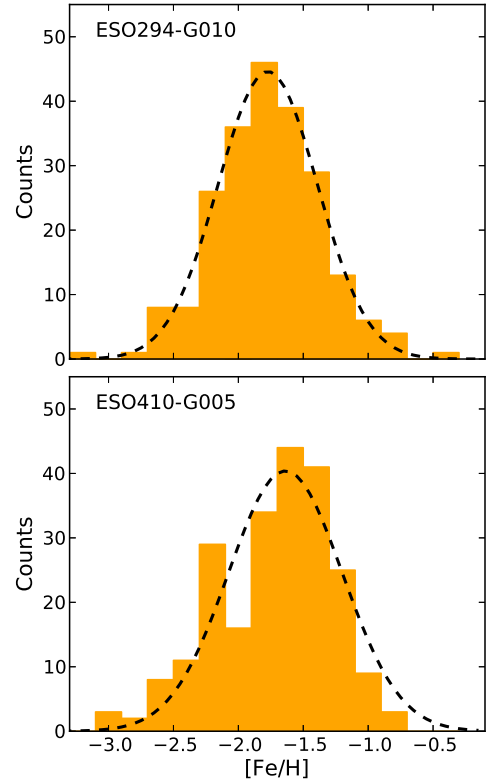


FIG. 10.— The metallicity distribution functions (MDFs) of RRL candidates in ESO294-G010 and ESO410-G005. The dashed lines indicate a Gaussian fit to these data. The best-fit Gaussians yield a mean of $[Fe/H] = -1.77$ and a standard deviation of 0.38 dex for ESO294-G010, and for ESO410-G005 these value become $[Fe/H] = -1.64$ and 0.44 dex.

stars exhibits a slightly lower metallicity peak as compared to that of the ESO410-G005 RRab stars. The mean metallicities estimated from the best-fit Gaussians to the MDFs are $\langle [Fe/H] \rangle = -1.77 \pm 0.03$ (sem) for ESO294-G010, and, $\langle [Fe/H] \rangle = -1.64 \pm 0.03$ (sem) for ESO410-G005 respectively. The uncertainties shown as sem here represent the standard errors of the mean values. The systematic errors are likely larger and closer to ~ 0.2 dex as demonstrated by Jeffery et al. (2011).

To better understand the properties of the RR Lyrae populations in these two dTrans galaxies, we now compare the RR Lyrae MDFs with those of the RGB stars. We construct MDFs of the RGB stars for both ESO294-G010 and ESO410-G005 by interpolating (Sarajedini & Jablonka 2005) within a set of Dartmouth isochrones (Dotter et al. 2008) that were generated to have metallicity values ranging from -2.5 to +0.5 dex at a fixed age of 12.5 Gyr. We used three values of $[\alpha/Fe] = 0.0, 0.2$, and 0.4 dex to gauge the effects of α element enhancement on the overall shape of the RGB MDF. For each galaxy, the RGB stars were selected within a magnitude range of $I_{TRGB} < I < 25$ (i.e. $I_{TRGB, ESO294} = 22.33$; $I_{TRGB, ESO410} = 22.36$, see the next section for the details). To account for interstellar extinction, reddening values of $E(B-V) = 0.006$ and 0.014 for ESO294-G010 and ESO410-G005 were adopted respectively from the

Galactic extinction map of Schlegel, Finkbeiner & Davis (1998).

Figure 11 illustrates the resulting MDFs of the RGB stars compared to those of the RR Lyrae stars. The MDFs are normalized to have the same total counts. In general, the overall shapes of the resultant RGB MDFs are not Gaussian but tend to be skewed toward lower abundances. We also see that the MDFs of the RGB stars are affected by the assumed values of α element ratio in the sense that higher the α element enhancement, the lower the overall metallicity. For ESO294-G010, the RRL stars appear to have a lower mean metal abundance as compared to the RGB stars at $[\alpha/Fe] = 0.0$ and 0.2 dex while the MDFs of these two stellar populations agree fairly well at $[\alpha/Fe] = 0.4$. In contrast with ESO294-G010, the metallicities of the RRL and RGB stars in ESO410-G005 generally agree well with each other except for where $[\alpha/Fe] = 0.4$ dex.

As seen from the CMDs of these two galaxies, their RGB stars exhibit a broad range in $(V-I)$ colors and noticeable features of intermediate age ($1 < \text{age} < 10$ Gyr) populations. It is worth mentioning here that Rejkuba et al. (2011) demonstrate that using the locations of RGB stars relative to a grid of standard RGB sequences with different metallicities in order to estimate the metal abundance of a diverse stellar population can lead to systematic effects. In particular, a metallicity bias of $0.1 - 0.2$ dex in the metal-poor direction can be introduced by age shifts from 12 Gyr to 8 Gyr, and this can cause a metallicity distribution to be skewed to the metal-poor end.

The comparisons presented above suggest that the RR Lyrae MDFs may be more reliable for studying the early chemical enrichment history of dwarf galaxies because RR Lyrae stars are not subject to the age-metallicity degeneracy, and the overall shape of the RRL MDF is not as significantly influenced by an assumed value of the $[\alpha/Fe]$ ratio as compared with MDFs generated using RGB stars. As a result, our estimates of the mean metallicities of type-ab RR Lyrae stars are free from the metal-poor bias induced by intermediate-age stellar populations; furthermore, the handful number of RR Lyrae candidates within the empirical instability strips in each target galaxy greatly reduces possible bias in the obtained metallicity values due to the evolutionary effects of these pulsation HB stars from the zero age HB (ZAHB). Therefore, we consider our metallicity estimates to be faithful to the purely ancient stellar populations in ESO294-G010 and ESO410-G005.

Now we turn our attention to whether the metallicities of the RRab samples show any radial trends throughout our target dTrans. Previously a metallicity gradient has been reported for the RR Lyrae stars in Tucana, one of the Milky Way dTrans in the sense that the more luminous, longer period (i.e. more metal-poor) RR Lyrae variables tend to be located at larger distances from the galactic center as compared to the fainter, shorter period (i.e. more metal-rich) RR Lyraes (Bernard et al. 2008). This phenomenon indicates that such a metallicity gradient should have occurred in a very early stage of evolution of this isolated dTran.

We examine the spatial distributions of our RRab samples in the fields of ESO294-G010 and ESO410-G005 in order to see if any radial trends similar to the case of

Tucana exist in these Sculptor group dTrans. To do this, we divide our RRab samples into three groups [i.e. metal-rich ($[Fe/H] > \langle [Fe/H] \rangle + 0.2$ dex), metal-poor ($[Fe/H] < \langle [Fe/H] \rangle - 0.2$ dex), and metal-intermediate ($\langle [Fe/H] \rangle - 0.2 < [Fe/H] < \langle [Fe/H] \rangle + 0.2$)] according to their metallicity ranges. Then we plot their locations on top of the elliptical isophote which corresponds to the visual extent of each dTran. From Figure 12, we are able to see that all three groups of RRab samples are well mixed with each other from the inner to the outer regions; therefore we conclude that there are no significant metallicity gradients among the RRab stars for both Sculptor Group dTrans. We also tested for a radial trend in the brightnesses of the RRab stars (see the bottom panels of Fig. 12). Similar to the previous test for metallicity, we do not see any systematic difference in their spatial distributions between luminous [$V < V(HB)$] and faint [$V > V(HB)$] groups. Further we checked the spatial distributions of the peculiar peak at around -2.2 dex (blue open circles) in the MDF of the ESO410-G005 RRab samples. As we can see from the figure, their spatial distributions do not show any peculiarity.

Most recently L13 presented a very detailed analysis of the spatial distributions of several different stellar populations in different age groups in these two dTrans. Their analysis revealed that the old stellar populations such as HB stars are more uniformly distributed throughout the galaxies, while the younger populations such as young blue main sequence stars or AGB stars are more concentrated to the inner regions of the dTrans. The results from our analysis of the spatial distributions of the RRab samples in ESO294-G010 and ESO410-G005 are consistent with those of L13 indicating that the physical and chemical processes in the early evolutionary phase of these Sculptor Group dTran seem to be different from the case of the isolated Milky Way dTran, Tucana.

3.4. Reddening and Distance

We adopt reddening values of $E(B-V) = 0.006$ and 0.014 for ESO294-G010 and ESO410-G005, respectively from the Galactic extinction map of Schlegel, Finkbeiner & Davis (1998) in the measurement of the distances to each galaxy. We are not able to estimate the line-of-sight reddenings toward the target galaxies using the minimum-light colors of the RRab stars because of the relatively low quality of the I-band light curves.

Along with the metallicity values of the individual RR Lyrae stars estimated in the previous sections, we now have the foundation for the calculation of accurate distances of our target galaxies. The mean V magnitude of the 219 RRab stars detected in ESO294-G010 is $\langle V(RR) \rangle = 26.95 \pm 0.01$ mag. The absolute V magnitudes of the individual RRab stars are calculated using the calibration given by Chaboyer (1999), $M_V = 0.23[Fe/H] + 0.93$. This gives a mean absolute V magnitude of $\langle M_V(RR) \rangle = 0.53 \pm 0.07$. The quoted error is the amount of uncertainty propagated from our measurement of the metal abundances of the RRab stars using the Alcock relation. By employing the extinction law, $A_V = 3.1E(B-V) = 0.019$ we obtained a distance modulus of $(m - M)_0 = 26.40 \pm 0.07$ mag which places ESO294-G010 at a distance of $\sim 1.9 \pm 0.1$ Mpc.

For ESO410-G005, the mean V magnitude of 225

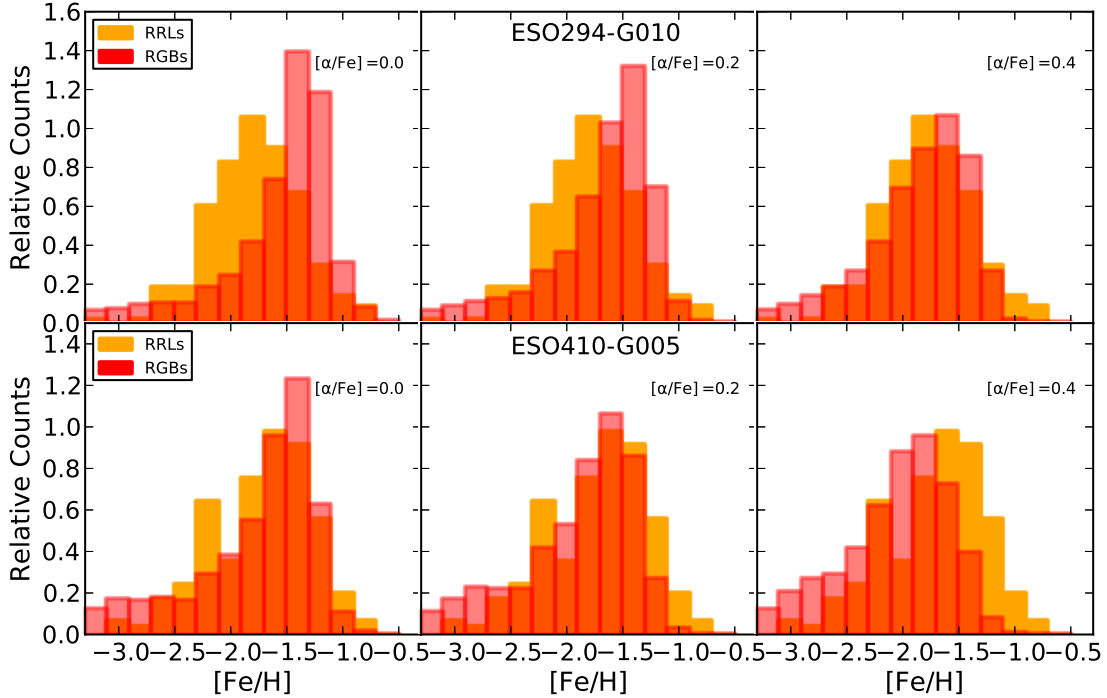


FIG. 11.— $[Fe/H]$ distributions for the RRab (orange) and RGB (red) stars in ESO294-G010 and ESO410-G005. The MDFs of the RGB stars were constructed using interpolation (Sarajedini & Jablonka 2005) within a grid of Dartmouth isochrones with metallicity values ranging from -2.5 to $+0.5$ dex at a fixed age of 12.5 Gyr.

RRab stars is $\langle V(RR) \rangle = 26.91 \pm 0.01$ mag. Applying once again the calibration of Chaboyer (1999) for the luminosity-metallicity relation for RRab stars, and the line-of-sight extinction $A_V = 0.043$, we obtain $\langle M_V(RR) \rangle = 0.53 \pm 0.07$ mag. This yields a distance modulus of $(m - M)_0 = 26.33 \pm 0.07$ mag which is equivalent to a distance of $\sim 1.9 \pm 0.1$ Mpc.

We have also calculated the distances of the two dTrans galaxies using the I-band magnitude of red giant branch tip (TRGB) in the VI CMDs in order to check the validity of our RR Lyrae distance estimate. We employed a weighted Sobel kernel $[-1, -2, 0, 2, 1]$ (Madore & Freedman 1995) to detect the TRGB of each galaxy (see Fig 13 & 14). This yields $I(TRGB) = 22.33 \pm 0.05$ mag for ESO294-G010 and 22.36 ± 0.05 for ESO410-G005. Applying the reddening ratio $E(V - I) = 1.38 E(B - V)$ provided by Tammann, Sandage & Reindl (2003), and $M_I^{TRGB} = -4.04 \pm 0.12$ (Bellazzini et al. 2001, 2004), we obtain $(m - M)_0 = 26.37 \pm 0.13$ and 26.38 ± 0.13 for ESO294-G010 and ESO410-G005 respectively. The errors represent the quadrature sum of the errors in the apparent and absolute I-band TRGB magnitudes. Our distance estimates for ESO294-G010 using two independent methods (RR Lyrae and TRGB) agree very well with each other. While ESO410-G005 shows ~ 0.1 mag discrepancy, this is still consistent within the margin allowed by the errors. The distances to these two galaxies derived in this study show excellent agreement with those measured in previous work such as L13, Da Costa et al. (2010), and the “Updated Nearby Galaxy Catalog” compiled by Karachentsev et al. (2013).

4. DISCUSSION

4.1. Star Formation History

The stellar populations of ESO294-G010 and ESO410-G005 share common features in the VI CMDs. However there also exist several noticeable differences in their CMDs indicating that these two dTrans systems might have experienced slightly different star formation histories. The main difference in the CMD features arises from the densities of YMS, BL, and blue HB (BHB) populations, in the sense that the YMS and BL stars in ESO410-G005 appear to be more populous than those in ESO294-G010, while the BHB feature seems relatively stronger in ESO294-G010 than in ESO410-G005. This indicates that ESO294-G010 apparently experienced reduced recent star formation (SF) as compared to ESO410-G005. Our assertion is nicely supported by the recent study of Weisz et al. (2011, W11 hereafter) on the star formation histories (SFHs) of 60 dwarf galaxies in the Local Volume. They used the same ACS/WFC imaging as in this study to extract the SFHs of ESO294-G010 and ESO410-G005 with the synthetic CMD routine developed by Dolphin (2002). W11’s results reveal that the two dTrans galaxies exhibit comparable star formation rates (SFRs) during the early epoch (look-back time > 10 Gyr) of their formation and evolution. Since then, ESO294-G010 has remained mostly dormant and has been sustaining very weak SFRs lower than its lifetime-averaged SFR, while ESO410-G005 shows a sudden enhancement of its SFRs within the most recent ~ 2 Gyr higher than its lifetime-averaged SFR. As a result, ESO294-G010 displays a bluer HB morphology and relatively weak features of luminous YMS and core He burning BL stars compared to ESO410-G005.

4.2. Early Chemical Evolution

According to the standard cosmological models of galaxy formation (White & Rees 1978; Hernquist &

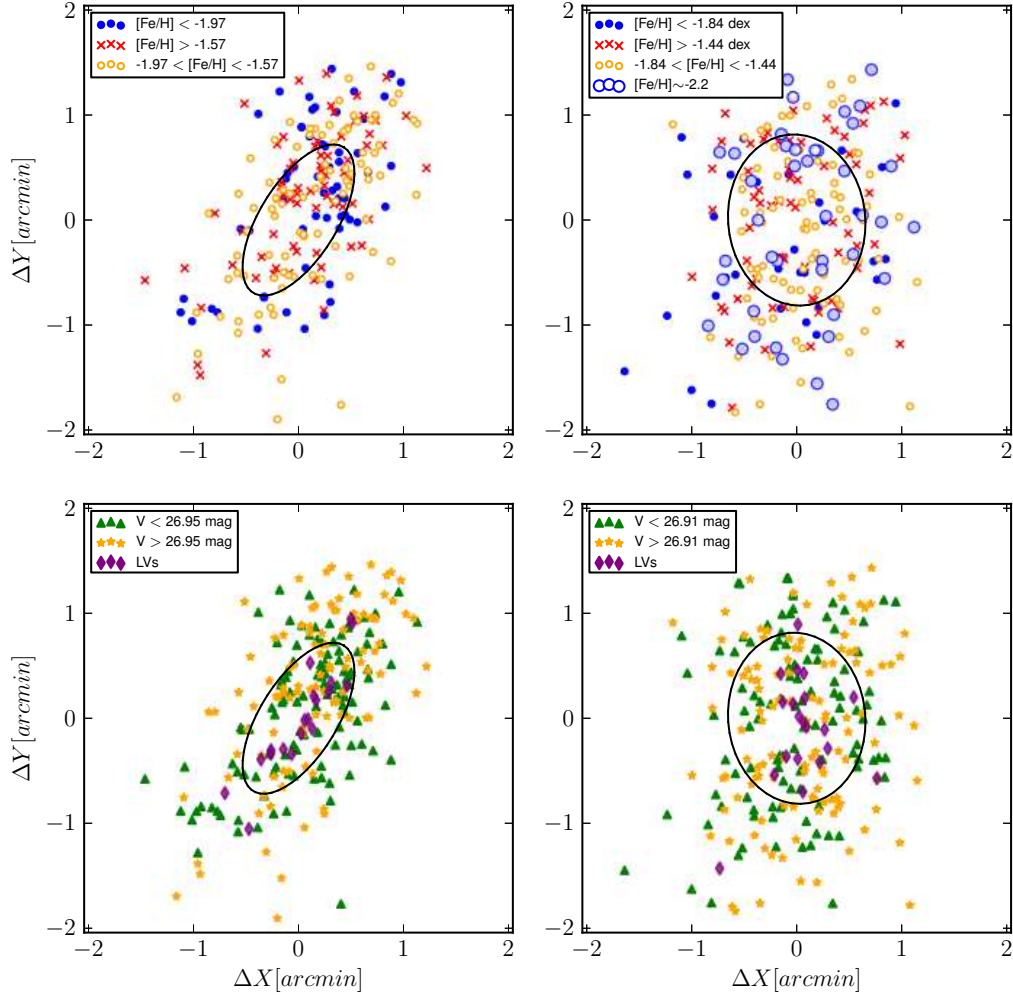


FIG. 12.— The spatial distribution of the RRab stars in each dTran. The ellipses represent the isophotes which correspond to the visual extents of each galaxy. Top panels show the spatial trend of the metal-rich (red cross), metal-poor (blue dot), and metal-intermediate (orange circle) groups. Bottom panels illustrate the spatial distributions of the luminous (green triangle; $V < V(HB)$) and faint (orange star; $V > V(HB)$) groups. The luminous variables (LVs; see section 3.2.1) are presented as purple diamonds showing that these stars are more centrally concentrated and aligned with the major axis of their host galaxy as compared to the RR Lyrae stars.

Quinn 1988, 1989; White & Frenk 1991), dwarf galaxies have likely formed through infall of primordial gas into a dark matter halo, and the subsequent star formation episodes determine the paths of their own chemical evolution as typical for galaxies. However the detailed patterns of the chemical evolution of these dwarf galaxies could be different from that of giant galaxies due to their shallower potential wells which lead to more efficient mixing and also make these systems more vulnerable to various kinds of environmental effects such as supernova driven galactic winds, ram pressure stripping, and tidal disruption. If this is the case, what would the early chemical evolution of dwarf galaxies in a low density environment such as the Sculptor group be like?

To answer this question, we analyze the RR Lyrae MDFs of our target dTrans systems using simple chemical enrichment models (Searle & Sargent 1972; Pagel

& Patchett 1975; Pagel 1997; Binney & Merrifield 1998) which depend on the initial heavy element abundance Z_0 of the star forming gas, effective nucleosynthetic yield y and loss or gain of star forming gas. The simplest version among the chemical evolution models is the closed-box model with an assumption of no inflow or outflow of gas during the evolution of the system. This model predicts a MDF of a stellar population produced from a star formation episode at a certain age with a gaussian-like exponential function,

$$\frac{dn}{dZ} \sim e^{-(Z-Z_0)/y}, \frac{dn}{d[M/H]} \sim \frac{Z-Z_0}{y} e^{-(Z-Z_0)/y}. \quad (3)$$

In these equations, the yield, y is equivalent to the mean metallicity of the system and $[M/H]$ is the total metal abundance of the system which accounts for the effect of alpha-capture element enhancement

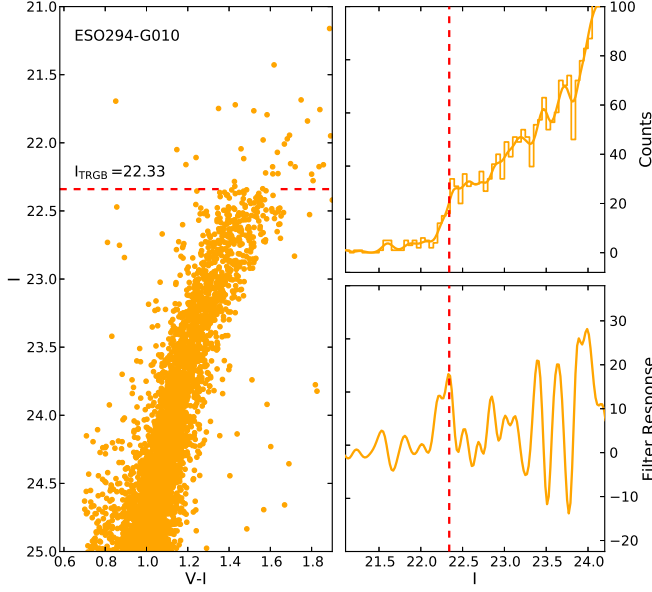


FIG. 13.— Our estimates of TRGB luminosity in the I-band for ESO294-G010. The right-lower panel illustrates the scaled response of a weighted Sobel kernel, $[-1, -2, 0, +2, +1]$ (Madore & Freedman 1995) on the I-band luminosity function of the RGB stars.

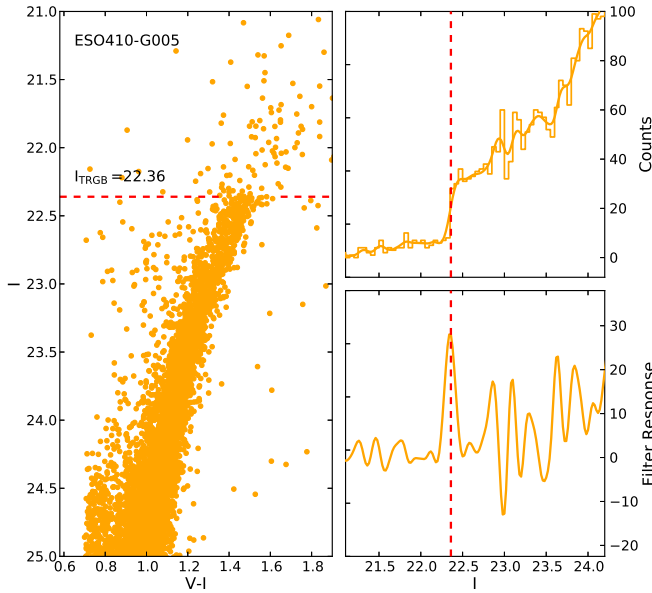


FIG. 14.— Same as Figure 13 but for ESO410-G005.

[i.e. $[M/H] = [Fe/H] + \log_{10}(0.638 \times 10^{[\alpha/Fe]} + 0.362)$; Salaris et al. 1993]. A number of studies (Tolstoy, Hill, & Tosi 2009 and references therein) have found that the old and metal-poor stars (age > 10 Gyr; $[M/H] < -1.6$ dex) in nearby dwarf galaxies exhibit the Galactic halo-like compositions with an enhanced alpha element ratio $\langle [\alpha/Fe] \rangle \sim 0.3$ dex. Therefore, assuming such an alpha element enhancement should be a reasonable approach. The red solid line in Figure 15 indicates the

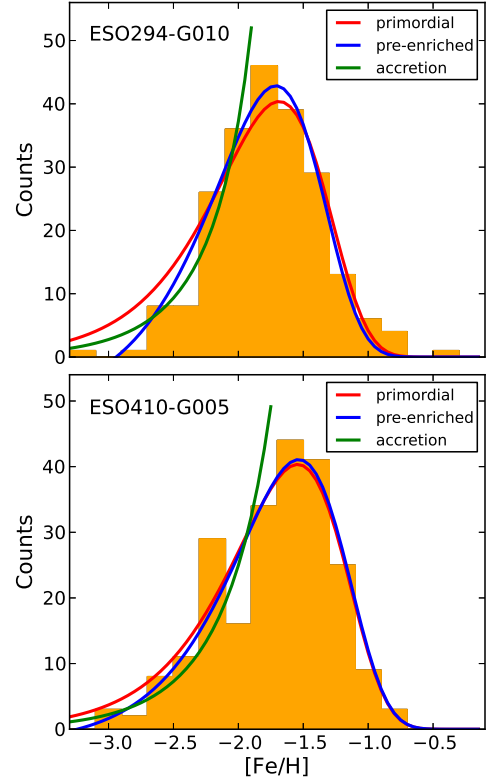


FIG. 15.— Our analysis of the RR Lyrae MDFs with several chemical evolution models. The green, blue, and red curves are the best-fit galactic chemical evolution models to the observed MDFs.

resulting fits of the simple closed box model with an assumption of a primordial abundance (e.g. $Z_0 = 0$) to our RR Lyrae MDFs of ESO294-G010 and ESO410-G005. We see that the predicted MDFs of the simple closed box model traces the observed MDFs reasonably well; however, in the case of ESO294-G010, the model MDF appears to slightly overestimate the number of metal-poor stars (e.g. $[Fe/H] < -2.2$ dex). This shortage of the low- Z stars, first recognized as the G-dwarf problem by van den Bergh (1962) and Schmidt (1963), is in fact a common issue for all types of galaxies (Binney & Merrifield 1998; Harris & Harris 2000; Pagel & Patchett 1975; Wheeler et al. 1989).

To compensate for this deficit of metal-poor stars, we adopt a pre-enrichment ($Z_0 \neq 0$) hypothesis for the star forming gas in which the dwarf galaxies were formed. The blue solid lines in Figure 15 illustrate the best-fit pre-enriched closed-box models. For ESO294-G010, a pre-enrichment model with an initial metal abundance of $Z_0 = 0.00004 \pm 4.45E-06$ (i.e. $[M/H]_0 \sim -2.7$ dex) and a chemical yield of $y = 0.00064 \pm 0.00003$ enhances the fit to the metal-poor tail of the observed MDF as compared to the simple closed box model. In the case of ESO410-G005, a pre-enriched system with an initial metal abundance of $Z_0 = 0.00002 \pm 4.43E-6$ (i.e. $[M/H]_0 \sim -3.0$ dex) and a yield of $y = 0.00097 \pm 0.00003$ agrees well with the observed RR Lyrae MDF featuring a comparable quality of fit to the simple closed box model.

The results of our analysis above naturally lead to the question as to the origin of the pre-enrichment source, and how the conditions in which the pre-enrichment was attained. It has been suggested by Truran & Cameron (1971) that such pre-enrichment in the star forming gas can be achieved through the process of “prompt initial enrichment” or “initial nucleosynthesis spike” which includes a preferential pre-galactic or proto-galactic event by high-mass stars during the very early phase of galaxy formation. Indeed our estimates of the initial metal abundances ($Z_{0,ESO294} = 0.00004$; $Z_{0,ESO410} = 0.00002$) from the best-fit pre-enrichment models are comparable to the initial cosmic metal enrichment levels ($10^{-6} < Z < 10^{-4}$) attained by the end products of population III stars (Schneider et al. 2002). In addition to this, it cannot be ruled out that the proto-galactic bodies of ESO294-G010 and ESO410-G005 could have been enriched by the products from more evolved systems of their nearest neighbor, NGC 55. Both hypotheses seem reasonable to explain the early chemical enrichment histories of our target dTrans galaxies in the low density environment of the Sculptor group.

Another approach to explain the metal-poor tail of the observed MDF is to lift the pure closed-box assumption by introducing an early phase gas inflow (or accretion) from the environment. The simplest form of this “accretion model” or “accreting-box” modification (Larson 1972; Timmes et al. 1995; Gibson & Matteucci 1997) assumes that the gas inflow rate is equals to the star formation rate of the system. This means that the mass of star forming gas M_g was a constant during the early epoch of galaxy formation. In these configurations, the predicted MDF is simplified to the following hyperbolic function (Binney & Merrifield 1998; Harris & Harris 2000; Sarajedini & Jablonka 2005),

$$\frac{dn}{dZ} \sim \frac{M_g}{y - Z}, \frac{dn}{d[M/H]} \sim M_g \frac{Z}{y - Z}. \quad (4)$$

In this formulation, during the early phase of evolution the system accumulates the heavy elements very efficiently with a high nucleosynthetic yield. As Z approaches y the dilution effect of the infalling gas starts to catch up to and ultimately squares off the accumulation rate of the heavy elements, thus the system reaches a steady state with no further global chemical enrichment. In Figure 15, we see that the observed metal-poor tails of the RR Lyrae MDFs ($[Fe/H] < -1.7$ dex) of both dwarf galaxies are very well described by our simple accretion models. From the best-fit models, we find $y = 0.00126 \pm 0.00003$ and 0.00315 ± 0.00007 for ESO294-G010 and ESO410-G005 respectively. As mentioned, this simple accretion model only accounts for the metal-poor stars formed during the very early epoch of the chemical evolution of the system. One of the most probable scenarios to explain the global pattern of the observed MDFs of the two dTrans galaxies is the so called “two phase scenario” of chemical evolution (Wyse & Gilmore 1993; Harris & Harris 2000; Sarajedini & Jablonka 2005): A bulk of stars attributed to the metal-poor tails of the MDFs formed in a very early gas infall phase. Once ESO294-G010 and ESO410-G005 were enriched enough to enter a steady state ($Z \rightarrow y$), both galaxies entered into the closed-box-like phase and the rest of the stars

associated with the remaining parts of the MDFs formed in the enriched gas deriving further chemical enrichment. Our analysis of the MDFs of RRL stars (age > 10 Gyr & age spread among RR Lyraes in a given stellar system does not exceed ~ 2 Gyr; Lee & Carney 1999) also suggests that this phase transition should occur within a short period of time.

4.3. Luminosity-Metallicity Relation

The luminosity-metallicity (or mass-metallicity) relation of galaxies (L-M relation) is one of the major predictions of chemical evolution models (van den Bergh 1962; Schmidt 1963; Searle & Sargent 1972; Erb et al. 2006), and it has been confirmed observationally by many studies. The current understanding of the L-M relation based on both theoretical and observational studies suggests that (1) the L-M relation exists among all kinds of galaxies within the Local Volume ($D < 10$ Mpc) regardless of their morphological types (Lequeux et al. 1979; Skillman et al. 1989; Zaritsky et al. 1994; Mateo 1998; Grebel et al. 2003, G03 hereafter; Salzer et al. 2005); (2) the L-M relation also exists among galaxies at intermediate redshift (i.e. $0.4 < z < 1.0$), and it seems that the L-M relation evolves over cosmological time in the sense that the slope at lower redshifts tends to be flatter than that at higher redshifts (i.e. The metallicity refers to the oxygen nebular emission, $12 + \log(O/H)$ in this case; Savaglio et al. 2005; Kobulnicky & Koo 2000; Kobulnicky et al. 2003; Kobulnicky & Kewley 2004; Maier et al. 2004; Shapley et al. 2005). The L-M relation for the old stellar populations of dwarf satellite galaxies in the Local Group and its neighbors is well established by using mean stellar $[Fe/H]$ -values which are based on both spectroscopic and photometric measurements for old RGB stars (see Figure 1. of G03). This L-M relation for nearby galaxies becomes not only a very useful analytical tool for understanding the fundamental differences and a possible evolutionary link between satellite galaxies with different morphological types, but also a basic ladder for the proper interpretation of the L-M relations at high redshifts.

With the mean metal abundances of the purely ancient stellar populations measured in section 3.3 by using the periods and amplitudes of the RRL stars, we plot ESO294-G010 and ESO410-G005 on the L-M relation of the nearby galaxies in Figure 16. The sample of the known nearby galaxies within a distance of $D \sim 2$ Mpc has been collected from the seminal work of G03 and the latest nearby galaxy catalog of Karachentsev et al. (2013; K13 hereafter). Our compilation (see Table 5) includes the recently discovered ultra-faint dwarf systems (uFds) around the Milky Way, and faint Andromeda dwarf galaxies (Willman et al. 2005a,b; Belokurov et al. 2006; Zucker et al. 2004, 2006a,b, 2007; Irwin et al. 2007, 2008; Walsh, Jerjen & Willman 2007; McConnachie et al. 2008; Martin et al. 2009; Richardson et al. 2011; Bell et al. 2011; Slater et al. 2011), which yields a total of 79 sample dwarf satellite galaxies. We use integrated K-band luminosity (L_K) values (adopted from Table 2 of K13) as the abscissa instead of using absolute V or B band magnitudes because the L_K is a better tracer for the total mass of a given galaxy (Drory et al. 2004).

From Figure 16, we see that all nearby galaxies, from luminous dEs (*red triangle*) to uFds (*blue square*), fall

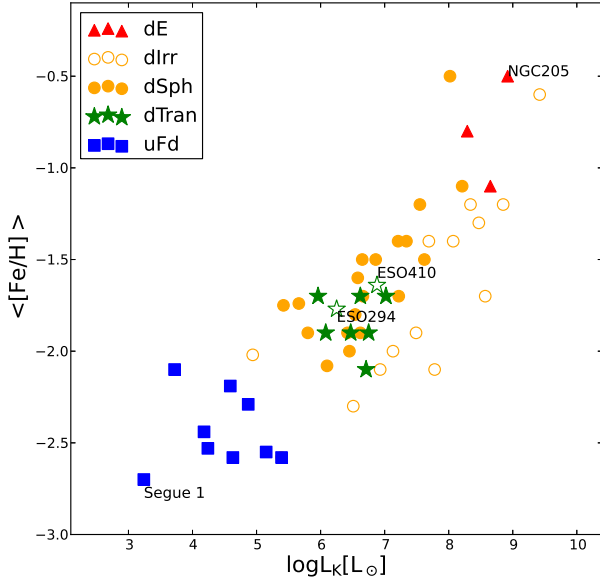


FIG. 16.— Luminosity–Metallicity (L–M) relation for Local Group dwarf galaxies. The data were obtained from the compilation of G03 for the canonical dwarf satellites. For the uFd systems, the data come from the recent work of Norris et al. (2010). ESO294–G010 and ESO410–G005 are shown as open star symbols. The M_V –metallicity relation appears to be very well established from the brightest dE, NGC 205, to the faintest MW satellite, Segue 1. Both dTran in the Sculptor Group trace the average L–M relation of the Local Group dSph galaxies. The typical error in the mean metallicity is about ~ 0.3 – 0.4 dex.

along the typical trend of the L–M relation - more luminous galaxies tend to be more metal-rich. Noticeable separations between dSphs (*orange dots*) and dIrrs (*orange circles*) are also observed in the sense that the dSphs appear to have higher metal abundances as compared to the dIrrs at the same luminosity level. This implies that at the early epochs of formation (age > 10 Gyr), the dSphs should have relatively more active star formation (SFs). As a result, the early chemical enrichment in the dSphs becomes much faster and efficient than in the dIrrs. This scenario of the early SF enhancement in the dSphs is echoed by the work of W11. Using the synthetic CMD analysis (Dolphin 2002), they have drawn the average cumulative SFs for five different morphological types (dSph, dIs, dTrans, dSpirals, and dTidals; see Figure 6 of W11). They have shown that on average the dSphs build up the bulk of their stellar populations (i.e. almost 65 – 70 % of their stellar masses) at the very earliest epochs of their formation $z > 2$ (i.e. age > 10 Gyr), while star formation in the dIrrs remains at the ~ 50 % level during the same epochs. This fundamental difference between the dSphs and dIrrs in their early star formation and chemical enrichment histories has raised serious doubts about the scenario which involves the morphological transformation dIrrs into dSphs by certain gas removal processes (G03). The locations of our target dTran galaxies ESO294–G010 and ESO410–G005 in the L–M relation agree with the typical trend of the other dTran systems (*green star*) such as Phoenix, Tucana, Cetus, LGS 3, KKR 25, DDO 210, and Antlia. Within a luminosity range of $5 < \log(L_K/L_\odot) < 7.5$, the L–M

relation of the sample dTran appears to show a closer resemblance to that of the canonical dSphs than dIrrs. In this regard, it has been suggested that a bulk of the dTran galaxies can be considered to be “*present – day progenitors*” of the dSph galaxies if the recent star formation of dTran galaxies were largely suppressed by rapid gas loss (G03).

4.4. Galaxy Environments

The most pivotal differences between dTran and dSphs galaxies might be the degree of recent star formations (SFs) and the local density environments where these galaxies formed and have been evolving. The morphology–density relation of galaxies in the Local Universe ($z \sim 0$) has revealed how different types of galaxies tend to be arranged in cluster environments, and provides important clues about how cluster/group environments affects the gas content and global SFR in the galaxy members. In general, gas-deficient early-type galaxies and bulge-dominated lenticular galaxies are preferentially located in the central, densest areas of galaxy clusters. Meanwhile, disk-dominated late-types galaxies (i.e. spirals and irregulars) tend to be more sparsely distributed in the outer regions of these clusters. The morphology–density relation appears to be a ubiquitous phenomenon in cluster environments regardless of their shapes and richness (van der Wel et al. 2010, and references therein).

Likewise, similar patterns of these morphological segregations have been observed among the dwarf satellite galaxies in the Local Group and other nearby galaxy groups. Figure 17 illustrates the H I gas content of our sample of dwarf galaxies normalized by their K-band luminosity as a function of the tidal index Θ_5 . This is basically the same plot as in the 2nd panel of the Fig 16 in K13, but for our 79 volume limited ($D_\odot < 2$ Mpc) sample dwarf galaxies. We consider this ratio to be a proxy of the gas fraction of the galaxy with respect to its total mass. This is a reasonable approximation not only because the K-band luminosity is an excellent tracer for the total mass of the galaxy but also the M/L values of galaxies in the K-band vary by only a factor of two across a wide range of galaxy morphologies and star formation histories (i.e. the M/L values in the B-band vary up to almost a factor of 10 in the nearby dwarf galaxy samples; Drory et al. 2004 and references therein).

K13 have provided the formula for the tidal index Θ_5 in the following form,

$$\Theta_5 = \log \left(\sum_{n=1}^5 M_n / D_{in}^3 \right) - 10.96, \quad (5)$$

where D_{in} is the spatial distance of a neighboring galaxy and M_n is its mass. The Θ_5 is a measure of the tidal force strength on a given galaxy exerted by the five most influential neighbors. Thus, it can be a robust estimate for the local tidal field strength. In this definition, the high positive Θ_5 values indicate a galaxy residing in a dense environment, and the negative values of Θ_5 represent isolated galaxies or galaxies in a very low density environment.

In Figure 17, we see a clear morphological segregation by local density environment and gas fraction in the senses like the following: (1) dIrr galaxies are the most

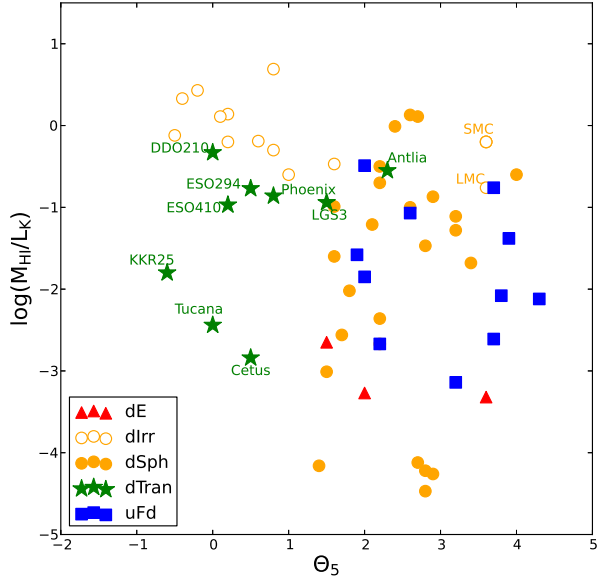


FIG. 17.— The H I gas content (i.e. the H I mass, M_{HI} normalized by K-band luminosity) plotted vs the tidal index, Θ_5 . The Θ_5 is a measure of tidal force strength on a given galaxy exerted by the five most influential neighbors. The high positive Θ_5 values indicate a galaxy residing in a dense environment, and the negative values of Θ_5 represent isolated galaxies or galaxies in a very low density environment. The majority of gas-rich dIrr galaxies tend to have lower tidal indices except for the LMC/SMC pair, while dSph/uFd/dE galaxies have predominantly high positive values (i.e. There are no early-type dwarf satellites having a Θ_5 value less than 1).

gas-abundant systems and there are no dIrrs with a gas fraction M_{HI}/L_K less than 0.1; (2) with the exception of which is known to be one of the closest neighboring galaxy groups the LMC/SMC pair ($\Theta_5 \sim 3.5$) and IC 10 ($\Theta_5 \sim 1.6$), the majority of the dIrr galaxies are mostly isolated in low density environments ($\Theta_5 < 1$). Together with their unusually high 3D velocities ($v_{LMC} = 378 \pm 18$ km s $^{-1}$; Kallivayalil et al. 2006) this could be another piece of evidence supporting the idea that the LMC/SMC pair may not be a canonical satellite system of the Milky Way but an infalling intruder which might be experiencing its first passage around the Milky Way (Besla et al. 2007); and (3) similar to the dIrr galaxies, most dTran galaxies are also found to be isolated but in general they have lower H I gas fractions as compared to the dIrrs.

All dSph, uFd and three dE (M32, NGC 205 and NGC 185) galaxies in our sample have relatively high tidal index values $\Theta_5 > 1$ indicating that these galaxies have been subjected to relatively higher local tidal fields (i.e. they are located within a galactocentric distance of $D \sim 200$ kpc to their giant hosts, Milky Way or M31) than the dTran and dIrrs galaxies. In terms of the gas content, some of the dSph systems such as Carina, Leo I, Sextans, Draco, Sag dSph, and NGC 147 exhibit the lowest H I gas fractions [$\log(M_{HI}/L_K) < -4$]; however, the rest of the early-type dwarfs are not completely gas-deficient but appear to have a wide range of H I gas fractions comparable to the levels of the dTran galaxies. Along with the difference in the local density environments, another conspicuous distinction between

dSphs and dTran seems to be the degree of recent SF. According to W11, within the most recent 1 Gyr, the dSph galaxies exhibit largely suppressed SFRs relative to those of dTran systems. Their estimates of the mean SFHs indicate that the typical dSph and dTran galaxies formed $\sim 2\%$ and 4% of their total stellar mass respectively within the last 1 Gyr.

This sudden drop in the recent SFRs of the dSphs might be due to a rapid gas loss which is a quite plausible process in the high local density environments in which these dSphs reside. Similar phenomena have been observed for many larger galaxy group/cluster environments in the Local Universe ($z \sim 0$). Recent star formation in galaxies located in denser regions appear to be largely quenched, and these galaxies tend to be more early-types and red (Oemler 1974; Davis & Geller 1976; Dressler 1980; Postman & Geller 1984; Wetzel, Tinker & Conroy 2012). This implies that the effects of environment on galaxy evolution operate in a similar fashion even in the low density environments of the LG and its neighboring groups (i.e. the Sculptor/Maffei groups).

5. SUMMARY AND CONCLUSION

We have presented an extensive analysis of the RR Lyrae stars in two transition type Sculptor group dwarf galaxies, ESO294-G010 and ESO410-G005. Based on the properties of the RR Lyrae stars we present the following results.

1. We have detected numerous RR Lyrae candidates in both ESO294-G010 ($N_{ab} = 219$) and ESO410-G005 ($N_{ab} = 225$). Based on the Bailey diagrams, the characteristics of the RR Lyrae stars in these two Sculptor group dTran appear to follow the typical trend of the RR Lyrae populations of Local Group dwarf satellite galaxies.
2. We construct the MDFs of the RRab stars using the period-amplitude-[Fe/H] relationship of Alcock et al. (2000). The mean metallicities estimated from the best-fit Gaussians to the MDFs are $\langle [Fe/H] \rangle = -1.77 \pm 0.03$ (sem) for ESO294-G010, and $\langle [Fe/H] \rangle = -1.64 \pm 0.03$ (sem) for ESO410-G005 respectively. Our results represent the metallicity values for purely ancient stellar populations in both dTran galaxies.
3. The distance of each dTran was calculated using the absolute V magnitudes of the RRab stars. We find $(m - M)_0 = 26.40 \pm 0.07$ mag for ESO294-G010 and $(m - M)_0 = 26.33 \pm 0.07$ mag for ESO410-G005. We have also calculated the distances of the two dTran using the I-band magnitudes of TRGBs in order to check the validity of our RR Lyrae distance estimates [$(m - M)_{0,ESO294} = 26.37$; $(m - M)_{0,ESO410} = 26.38$]. Our distance estimates for ESO294-G010 using two independent methods (RRLs and TRGB) agree very well with each other. In the case of ESO410-G005, there is a ~ 0.1 mag difference but this is consistent within the margin allowed by the errors.
4. We have compared the RR Lyrae MDFs for ESO294-G010 and ESO410-G005 with several chemical evolution models. For both galaxies, the

shapes of the RR Lyrae MDFs are nicely described by pre-enrichment models. This suggests two possible channels for the early chemical evolution of these Sculptor group systems: 1) The ancient stellar populations of our target dwarf galaxies might have formed from the star forming gas which was already enriched through “prompt initial enrichment” or an “initial nucleosynthesis spike” caused by the very first massive stars, or 2) This pre-enrichment state might have been achieved by the end products from more evolved systems of their nearest neighbor, NGC 55. We also fit a simple accretion model to the RR Lyrae MDFs of each galaxy. The gas infall hypothesis seems to explain the metal-poor tail of the RR Lyrae MDFs indicating that we cannot completely rule out the role of gas accretion on the early chemical evolution of the dTrans.

5. The L-M relation of our target dTrans ESO294-G010 and ESO410-G005 follow the typical trend of other Local Group dTrans galaxies, such as Phoenix, Tucana, Cetus, LGS 3, KKR 25, DDO 210, and Antlia. Within a luminosity range of $5 < \log(L_K/L_\odot) < 7.5$, the L-M relation of the sample dTrans appear to show a closer resemblance to that of the canonical dSphs than dIrrs. This suggests that the bulk of the dTran galaxies can be considered as “*present – day progenitors*” of the dSph galaxies if the recent star formation of dTrans

galaxies has been largely suppressed by rapid gas loss (G03).

6. Our examination of the H I gas content as a function of the tidal index Θ_5 for 79 volume limited ($D_\odot < 2$ Mpc) dwarf galaxies reveals a clear morphological segregation, in the sense that gas-deficient dSphs tend to be located in dense areas while most gas-rich dIrrs (except LMC/SMC pairs) are isolated. Similar to the dIrr galaxies, most dTran galaxies are also found to be isolated but in general they have lower H I gas fractions as compared to the dIrrs. Our analysis supports the idea that the morphology-density relation appears to be a ubiquitous phenomena in cluster environments regardless of their shapes and richness (van der Wel et al. 2010, and references therein), and the environmental effects on galaxy evolution operate in a similar fashion even in such low density environments of the Local Group or its neighboring groups.

We are grateful to the anonymous referee whose comments and suggestions improved the clarity and quality of this paper. This work was supported by KASI-Carnegie Fellowship Program jointly managed by Korea Astronomy and Space Science Institute (KASI) and the Observatories of the Carnegie Institution for Science.

REFERENCES

- Alcock, C., et al. 2000, *AJ*, 119, 2194
- Binney, J., & Merrifield, M. 1998, *Galactic Astronomy* (Princeton, NJ : Princeton University Press)
- Bell, E. F., Slater, C. T., & Martin, N. F. 2011, *ApJL*, 742, 15
- Bellazzini, M., Ferraro, F. R., & Pancino, E. 2001, *ApJ*, 556, 635
- Bellazzini, M., Ferraro, F. R., Sollima, A., Pancino, E., & Origlia, L. 2004, *A&A*, 424, 199
- Belokurov, V. et al. 2006, *ApJL*, 647, 111
- Bernard, E. J. et al. 2008, *ApJ*, 678L, 21
- Bernard, E. J. et al. 2009, *ApJ*, 699, 1742
- Besla, G., Kallivayalil, N., Hernquist, L., Robertson, B., Cox, T. J., van der Marel, R. P., & Alcock, C. 2007, *ApJ*, 668, 949
- Bouchard, A., Da Costa, G. S., Jerjen, H., & Ott, J. 2005, in *IAUC. 198, Near-Field Cosmology with Dwarf Elliptical Galaxies* (Les Diablerets, Switzerland), 255
- Cacciari, C., Corwin, T. M., & Carney, B. W. 2005, *AJ*, 129, 267
- Castellani, V. & Quarta, M. L. 1987, *A&AS*, 71, 1
- Chaboyer, B. 1999, in Heck A., Caputo F., eds, *Astrophysics and Space Science Library Vol. 237, Post-Hipparcos Cosmics Candles*. Kluwer, Dordrecht, p.111
- Clement, C. M., & Rowe, J. 2000, *AJ*, 120, 2579
- Da Costa, G. S., Rejkuba, M., Jerjen, H., & Grebel, E. K. 2010, *ApJL*, 708, 121
- Davis, M., & Geller, M. J. 1976, *ApJ*, 208, 13
- de Vaucouleurs, G., de Vaucouleurs, A., Corwin, H. G., Jr., Buta, R. J., Paturel, G., & Fouqu, P. 1991, *Third Reference Catalogue of Bright Galaxies. Volume I: Explanations and references. Volume II: Data for galaxies between 0^h and 12^h. Volume III: Data for galaxies between 12^h and 24^h.* (New York, NY (USA) : Springer), ISBN 0-387-97552-7
- Dolphin, A. E. 2000, *PASP*, 112, 1383
- Dolphin, A. E. 2002, *MNRAS*, 332, 91
- Dolphin, A. E. et al. 2004, *AJ*, 127, 875
- Dotter, A., Chaboyer, B., Jevremovi?, D., Kostov, V., Baron, E., & Ferguson, J. W. 2008, *ApJS*, 178, 89
- Dressler, A. 1980, *ApJ*, 236, 351
- Drory, N., Bender, R., Feulner, G., Hopp, U., Maraston, C., Snigula, J., & Hill, G. J. 2004, *ApJ*, 608, 742
- Erb, D. K., Shapley, A. E., Pettini, M., Steidel, C. C., Reddy, N. A., & Adelberger, K. L. 2006, *ApJ*, 644, 813
- Gallart, C. et al. 2004, *ApJ*, 127, 1486
- Gibson, B. K., & Matteucci, F. 1997, *MNRAS*, 291, 8
- Grebel, E. K., Gallagher, J. S., III, & Harbeck, D. 2003, *AJ*, 125, 1926
- Guldenschuh, K. A., et al. 2005, *PASP*, 117, 721
- Harris, G. L. H., & Harris, W. E. 2000, *AJ*, 120, 2423
- Hernquist, L., & Quinn, P. J. 1988, *ApJ*, 331, 682
- Hernquist, L., & Quinn, P. J. 1989, *ApJ*, 342, 1
- Irwin, M. J. et al. 2007, *ApJL*, 656, 13
- Irwin, M. J., Ferguson, A. M. N., Huxor, A. P., Tanvir, N. R., Ibata, R. A., & Lewis, G. F. 2008, *ApJL*, 676, 17
- Jeffery, E. J. et al. 2011, *AJ*, 141, 171
- Jerjen, H., Freeman, K. C., & Binggeli, B. 1998, *AJ*, 116, 2873
- Kallivayalil, N., van der Marel, R. P., Alcock, C., Axelrod, T., Cook, K. H., Drake, A. J., & Geha, M. 2006, *ApJ*, 638, 772
- Karachentsev, D., et al. 2003, *A&A*, 404, 93
- Karachentsev, I. D., Karachentseva, V. E., Huchtmeier, W. K., & Makarov, D. I. 2004, *AJ*, 127, 2031
- Karachentsev, I. D., Makarov, D. I., & Kaisina, E. I. 2013, *AJ*, 145, 101
- Kirby, E. N., Simon, J. D., Geha, M., Guhathakurta, P., & Frebel, A. 2008, *ApJL*, 685, 43
- Kobulnicky, H. A., & Koo, D. C. 2000, *ApJ*, 545, 712
- Kobulnicky, H. A. et al. 2003, *ApJ*, 599, 1006
- Kobulnicky, H. A., & Kewley, L. J. 2004, *ApJ*, 617, 240
- Larson, R. B. 1972, *Nature*, 236, 21
- Layden, A. C. 1998, *AJ*, 115, 193
- Lee, J.-W., & Carney, B. W. 1999, *AJ*, 118, 1373
- Lequeux, J., Peimbert, M., Rayo, J. F., Serrano, A., & Torres-Peimbert, S. 1979, *A&A*, 80, 155
- Lianou, S., Grebel, E. K., Da Costa, G. S., Rejkuba, M., Jerjen, H., & Koch, A. 2013, *A&A*, 550, A7 (L13)
- Madore, B. F., & Freedman, W. L. 1995, *AJ*, 109, 1645
- Maier, C., Meisenheimer, K., & Hippelein, H. 2004, *A&A*, 418, 475
- Mackey, A. D., & Gilmore, G. F. 2003, *MNRAS*, 343, 747

- Martin, N. F. et al. 2009, *ApJ*, 705, 758
- Mateo, M. L. 1998, *ARA&A*, 36, 435
- Matteucci, F. 2012, *Chemical Evolution of Galaxies* (Heidelberg: Springer)
- McConnachie, A. W. et al. 2008, *ApJ*, 688, 1009
- Norris, J. E. et al. 2010, *ApJ*, 723, 1632
- Oemler, A. J. 1974, *ApJ*, 194, 10
- Pagel, B. E. J., & Patchett, B. E. 1975, *MNRAS*, 172, 13
- Pagel, B. E. J. 1997, *Nucleosynthesis and Chemical Evolution of Galaxies* (Cambridge, UK: Cambridge University Press), ISBN 0521550610
- Postman, M. & Geller, M. J. 1984, *ApJ*, 281, 95
- Pritzl, B. J., Armandroff, T. E., Jacoby, G. H., & Da Costa, G. S. 2005, 129, 2232
- Rejkuba, M., Harris, W. E., Greggio, L., & Harris, G. L. H. 2011, *A&A*, 526, 123
- Richardson, J. C. et al. 2011, *ApJ*, 732, 76
- Sarajedini, A., & Jablonka, P. 2005, *AJ*, 130, 1627
- Sarajedini, A., Barker, M. K., Geisler, D., Harding, P., & Schommer, R. 2006, *AJ*, 132, 1361
- Sarajedini, A., Yang, S.-C., Monachesi, A., Lauer, T. R., & Trager, S. C. 2012, *MNRAS*, 425, 1459
- Salaris, M., Chieffi, A., & Straniero, O. 1993, *ApJ*, 414, 580
- Salzer, J. J., Lee, J. C., Melbourne, J., Hinz, J. L., Alonso-Herrero, A., & Jangren, A. 2005, *ApJ*, 624, 661
- Savaglio, S. et al. 2005, *ApJ*, 635, 260
- Schmidt, M. 1963, *ApJ*, 137, 758
- Schneider, R., Ferrara, A., Natarajan, P., & Omukai, K. 2002, *ApJ*, 571, 30
- Searle, L., & Sargent, W. L. W. 1972, *ApJ*, 173, 25
- Schlegel, D. J., Finkbeiner, D. P., & Davis, M. 1998, *ApJ*, 500, 525
- Shapley, A. E. et al. 2005, *ApJ*, 626, 698
- Sirianni, M., Jee, M. J., Bentez, N., & et al. 2005, *PASP*, 117, 1049
- Skillman, E. D., Kennicutt, R. C., & Hodge, P. W. 1989, *ApJ*, 347, 875
- Slater, C. T., Bell, E. F., & Martin, N. F. 2011, *ApJL*, 742, 14
- Tamman, G. A., Sandage, A., & Reindl, B. 2003, *A&A*, 404, 423
- Timmes, F. X., Woosley, S. E., & Weaver, Thomas A. 1995, *ApJS*, 98, 617
- Tolstoy, E., Hill, V., & Tosi, M. 2009, *ARA&A*, 47, 371
- Truran, J. W., & Cameron, A. G. W. 1971, *Ap&SS*, 14, 179
- van den Bergh, S. 1962, *AJ*, 67, 486
- van der Wel, A., Bell, E. F., Holden, B. P., Skibba, R. A., Rix, H. 2010, *ApJ*, 714, 1779
- Walsh, S. M., Jerjen, H., & Willman, B. 2007, *ApJL*, 662, 83
- Weisz, D. R. et al. 2011, *ApJ*, 739, 5 (W11)
- Wetzell, A. R., Tinker, J. L., & Conroy, C. 2012, *MNRAS*, 424, 232
- Wheeler, J. C., Sneden, C., & Truran, J. W., Jr. 1989, *ARA&A*, 27, 279
- Willman, B. et al. 2005a, *AJ*, 129, 2692
- Willman, B. et al. 2005b, *ApJL*, 626, 85
- Willman, B. et al. 2011, *AJ*, 142, 128
- White, S. D. M., & Rees, M. J. 1978, *MNRAS*, 183, 341
- White, S. D. M., Frenk, C. S. 1991, *ApJ*, 379, 52
- Wyse, R. F. G., & Gilmore, G. 1993, in *ASP Conf Ser.* 48, *The globular clusters-galaxy connection*, ed. G. H. Smith, & J. P. Brodie (Santa Cruz, San Francisco, CA: ASP), 727
- Yang, S.-C., Sarajedini, A., Holtzman, J. A., & Garnett, D. R. 2010, *ApJ*, 724, 799 (Y10)
- Yang, S.-C., & Sarajedini, A. 2012, *MNRAS*, 419, 1362 (YS12)
- Zaritsky, D., Kennicutt, R. C., Jr., & Huchra, J. P. 1994, 1994, *ApJ*, 420, 87
- Zinn, R. & West, M. 1984, *ApJS*, 55, 45
- Zorotovic, M. et al. 2010, *AJ*, 139, 357
- Zucker, D. B. et al. 2004, *ApJL*, 612, 121
- Zucker, D. B. et al. 2006a, *ApJL*, 643, 103
- Zucker, D. B. et al. 2006b, *ApJL*, 650, 41
- Zucker, D. B. et al. 2007, *ApJL*, 659, 21

TABLE 2
PULSATION PROPERTIES OF RR LYRAE STARS IN ESO294-G010

ID	RA (J2000)	Decl (J2000)	$\langle V \rangle$	$\langle V \rangle - \langle I \rangle$	Period (days)	Amp(V)	Note
RRab	WFC1 field						
31519	0:26:27.47	-41:51:54.93	27.086	0.548	0.5200	0.8116	
31435	0:26:28.37	-41:51:54.95	26.934	0.438	0.6760	1.0592	
26874	0:26:28.56	-41:52:12.85	26.759	0.394	0.6471	0.9721	
29750	0:26:29.03	-41:52:24.77	27.011	0.657	0.4951	1.0102	
32272	0:26:29.42	-41:50:51.19	27.193	0.633	0.5932	1.0251	
:	:	:	:	:	:	:	
RRc	WFC1 field						
32536	0:26:27.76	-41:52:09.32	26.940	0.265	0.3004	0.6436	
28014	0:26:28.65	-41:51:03.54	26.792	0.546	0.3060	0.4139	
29510	0:26:31.46	-41:51:35.01	26.812	0.318	0.3914	0.5809	
32861	0:26:31.94	-41:52:58.44	27.044	0.451	0.3699	0.4827	
27866	0:26:33.32	-41:51:34.42	26.729	0.434	0.3183	0.7197	bl
:	:	:	:	:	:	:	
RRab	WFC2 field						
23778	0:26:28.85	-41:49:57.87	26.870	0.600	0.6373	0.4490	
23713	0:26:30.13	-41:50:17.34	26.823	0.484	0.5887	0.6919	
25347	0:26:31.04	-41:50:02.74	27.107	0.685	0.6058	1.0376	
24215	0:26:31.34	-41:49:55.30	26.926	0.666	0.6529	0.7934	
24335	0:26:31.93	-41:50:41.47	27.007	0.429	0.5483	1.0382	bl
:	:	:	:	:	:	:	
RRc	WFC2 field						
23174	0:26:33.36	-41:50:29.40	26.832	0.568	0.3446	0.5975	
23720	0:26:34.14	-41:50:11.63	26.898	0.643	0.3781	0.4427	
25657	0:26:38.24	-41:49:48.61	27.108	0.605	0.4025	0.5852	

NOTE. — “bl” in the final column indicates *blend* objects.

** The full table will be available in a machine-readable format in the published version

TABLE 3
PULSATION PROPERTIES OF RR LYRAE STARS IN ESO410-G005

ID	RA (J2000)	Decl (J2000)	$\langle V \rangle$	$\langle V \rangle - \langle I \rangle$	Period (days)	Amp(V)	Note
RRab	WFC1 field						
27360	0:15:24.34	-32:10:42.23	26.983	0.518	0.5624	0.9455	
25183	0:15:25.04	-32:10:40.32	26.830	0.636	0.6718	0.6186	
25200	0:15:25.27	-32:11:25.31	26.824	0.462	0.6851	0.7559	
24100	0:15:25.34	-32:11:25.56	26.797	0.412	0.5933	1.1051	
27060	0:15:25.54	-32:11:31.52	26.926	0.412	0.5707	0.6277	
:	:	:	:	:	:	:	
RRc	WFC1 field						
24150	0:15:25.57	-32:11:24.13	26.684	0.218	0.3242	0.5591	
31623	0:15:27.96	-32:11:25.57	27.143	0.394	0.2895	0.4600	bl
24390	0:15:28.44	-32:10:58.97	26.759	0.574	0.2668	0.4252	
26141	0:15:28.54	-32:11:46.15	26.779	0.340	0.3460	0.7136	
23520	0:15:28.66	-32:11:17.69	26.791	0.690	0.4048	0.6748	
:	:	:	:	:	:	:	
RRab	WFC2 field						
18627	0:15:29.79	-32:09:45.39	26.987	0.622	0.5446	0.8530	
15681	0:15:30.19	-32:09:19.01	26.725	0.433	0.6162	0.9297	
18442	0:15:30.40	-32:10:05.50	26.794	0.478	0.6037	1.2543	
16370	0:15:30.52	-32:08:38.45	26.845	0.617	0.6592	1.1345	
20519	0:15:30.90	-32:09:56.61	26.950	0.597	0.6162	1.0357	
:	:	:	:	:	:	:	
RRc	WFC2 field						
19124	0:15:31.63	-32:10:15.45	26.809	0.479	0.3146	0.6532	
16185	0:15:31.65	-32:10:19.04	26.709	0.700	0.2195	0.6250	
19968	0:15:31.99	-32:10:28.29	26.958	0.479	0.3597	0.7719	bl
19264	0:15:33.55	-32:09:53.06	26.862	0.576	0.2885	0.5935	
16866	0:15:33.68	-32:10:26.99	26.783	0.667	0.3271	0.5668	bl
:	:	:	:	:	:	:	

NOTE. — “bl” in the final column indicates *blend* objects.

** The full table will be available in a machine-readable format in the published version

TABLE 4
PULSATION PROPERTIES OF LUMINOUS VARIABLES

ID	RA (J2000)	Decl (J2000)	$\langle V \rangle$	$\langle V \rangle - \langle I \rangle$	Period (days)	Amp(V)	Note
ESO294-G010	WFC1 field						
3817	0:26:32.12	-41:51:49.45	25.377	0.543	1.8274	1.0387	bl
14561	0:26:32.44	-41:52:24.09	26.038	0.393	0.4650	0.7667	
23638	0:26:32.62	-41:52:22.60	26.482	0.282	0.4418	0.5510	
21370	0:26:33.31	-41:51:35.21	26.521	0.561	0.5339	0.4820	bl
1660	0:26:33.52	-41:51:34.13	24.784	0.501	0.8735	0.3924	bl
5048	0:26:33.61	-41:51:47.51	25.492	0.483	1.4140	0.6971	bl
18994	0:26:33.68	-41:51:20.84	26.278	0.250	0.4283	0.5306	bl
19596	0:26:33.79	-41:51:22.39	26.378	0.480	0.5473	0.2845	bl
20461	0:26:33.80	-41:51:42.26	26.302	0.417	0.5473	0.7387	bl
1226	0:26:33.94	-41:51:13.44	24.503	0.511	1.9431	0.5900	bl
5366	0:26:34.24	-41:51:19.52	25.588	0.593	1.3464	0.7185	bl
15933	0:26:34.36	-41:51:51.62	26.204	0.416	0.5698	0.5743	bl
ESO294-G010	WFC2 field						
2754	0:26:32.62	-41:50:19.13	25.287	0.649	1.5201	0.6490	
2412	0:26:33.07	-41:50:47.32	24.933	0.390	1.1971	0.5833	bl
3249	0:26:33.21	-41:50:55.11	25.395	0.594	0.4683	0.2520	bl
10896	0:26:33.31	-41:50:53.40	26.136	0.482	0.7133	0.8989	bl
2432	0:26:33.69	-41:50:59.90	24.967	0.473	1.2844	1.1950	bl
14201	0:26:34.19	-41:51:00.50	26.209	0.485	0.6302	0.3131	bl
3942	0:26:34.74	-41:50:10.73	25.642	0.631	1.2321	0.7236	
ESO410-G005	WFC1 field						
6202	0:15:28.56	-32:11:31.48	25.707	0.540	0.9203	0.6795	
1756	0:15:29.54	-32:11:03.79	24.746	0.547	1.5094	1.2808	bl
2067	0:15:29.97	-32:11:11.94	24.902	0.523	0.9324	0.4800	bl
1409	0:15:30.29	-32:11:13.20	24.417	0.390	1.1129	0.4249	bl
2387	0:15:30.50	-32:10:52.73	25.025	0.523	0.7383	0.5900	bl
973	0:15:30.91	-32:10:55.99	24.268	0.419	1.7204	1.1464	bl
1959	0:15:31.10	-32:11:03.09	24.887	0.652	1.7143	0.5899	bl
2278	0:15:31.49	-32:10:53.14	25.039	0.538	1.2008	0.6843	bl
1147	0:15:31.85	-32:10:52.33	24.207	0.441	1.1759	0.6793	bl
2803	0:15:32.05	-32:10:51.68	25.159	0.630	1.2684	0.9685	bl
9037	0:15:32.71	-32:11:22.99	25.987	0.606	0.5413	0.5250	
1553	0:15:32.76	-32:10:57.75	24.590	0.447	1.0492	0.3652	bl
ESO410-G005	WFC2 field						
1413	0:15:32.33	-32:10:31.04	25.022	0.418	0.8278	0.4415	bl
1023	0:15:32.51	-32:10:18.59	24.694	0.412	0.7997	0.5748	bl
1105	0:15:32.78	-32:10:34.68	24.840	0.570	1.0211	0.5039	bl
1546	0:15:33.46	-32:10:51.05	25.130	0.477	1.0981	0.4714	bl
1923	0:15:33.61	-32:10:42.03	25.261	0.484	0.7039	0.3242	bl
6160	0:15:33.63	-32:09:17.19	26.044	0.486	0.6571	0.4327	bl
879	0:15:33.99	-32:10:22.82	24.603	0.476	1.0377	0.8358	

NOTE. — “bl” in the final column indicates *blend* objects.

TABLE 5
PHYSICAL PROPERTIES OF NEARBY DWARF SATELLITE GALAXIES

Object	RA (J2000)	Dec. (J2000)	D_{\odot}	M_B	$\langle [Fe/H] \rangle$	Ref	$\log M_{HI}$	$\log L_K$	Θ_5	Type
MW Group										
SMC	00 52 38.0	-72 48 01	0.06	-16.5	-1.20 ± 0.40	1	8.65	8.85	3.6	dIrr
Sculptor	01 00 09.4	-33 42 33	0.09	-9.8	-1.50 ± 0.50	1	5.39	6.86	2.8	dSph
Phoenix	01 51 06.3	-44 26 41	0.44	-9.6	-1.90 ± 0.40	1	5.22	6.08	0.8	dTran
Segue 2	02 19 16.0	+20 10 31	0.03	-2.3	-	-	-	3.88	3.8	uFd
Fornax	02 39 54.7	-34 31 33	0.14	-11.5	-1.20 ± 0.50	1	5.19	7.55	2.2	dSph
LMC	05 23 34.6	-69 45 22	0.05	-17.9	-0.60 ± 0.50	1	8.66	9.42	3.6	dIrr
Carina	06 41 36.7	-50 57 58	0.10	-9.0	-1.80 ± 0.30	1	2.32	6.54	2.8	dSph
UMa II	08 51 30.0	+63 07 48	0.03	-3.1	-2.44 ± 0.53	2	2.80	4.18	3.9	uFd
LeoT	09 34 53.4	+17 03 05	0.42	-6.7	-2.02 ± 0.54	4	5.63	4.94	0.8	dIrr
SexB	10 00 00.1	+05 19 56	1.36	-14.0	-2.10 ± 0.40	1	7.66	7.78	-0.5	dIrr
Segue 1	10 07 03.2	+16 04 25	0.02	-0.7	-2.70 ± 0.70	2	1.12	3.24	4.3	uFd
LeoI	10 08 26.9	+12 18 29	0.25	-11.0	-1.40 ± 0.50	1	3.18	7.34	1.4	dSph
SexA	10 11 00.8	-04 41 34	1.32	-13.9	-1.90 ± 0.40	1	7.82	7.49	-0.4	dIrr
Sextans	10 13 03.0	-01 36 52	0.09	-8.7	-1.90 ± 0.40	1	2.30	6.42	2.7	dSph
UMa I	10 34 52.8	+51 55 12	0.10	-4.8	-2.29 ± 0.50	2	3.80	4.87	2.6	uFd
Willman1	10 49 21.0	+51 03 00	0.04	-1.9	-2.10	5	2.96	3.72	3.7	uFd
LeoII	11 13 29.2	+22 09 17	0.21	-9.1	-1.60 ± 0.50	1	4.02	6.58	1.7	dSph
LeoV	11 31 09.6	+02 13 12	0.18	-3.8	-	-	2.88	4.46	1.9	uFd
LeoIV	11 32 57.0	-00 32 00	0.16	-4.2	-2.58 ± 0.72	2	2.78	4.63	2.0	uFd
ComaI	12 26 59.0	+23 54 15	0.04	-3.2	-2.53 ± 0.40	2	1.63	4.24	3.7	uFd
CVnII	12 57 10.0	+34 19 15	0.16	-4.1	-2.19 ± 0.54	2	4.10	4.59	2.0	uFd
CVnI	13 28 03.5	+33 33 21	0.22	-7.9	-2.08 ± 0.41	2	4.50	6.10	1.6	dSph
BootesIII	13 57 07.4	+26 46 30	0.05	-5.9	-	-	-	5.29	3.6	uFd
BootesII	13 58 00.0	+12 50 00	0.04	-1.9	-	-	1.62	3.70	3.8	uFd
BootesI	14 00 00.0	+14 30 00	0.07	-5.5	-2.55 ± 0.37	2	2.01	5.15	3.2	uFd
UMin	15 09 11.3	+67 12 52	0.06	-7.1	-1.90 ± 0.70	2	4.52	5.80	3.2	dSph
Hercules	16 31 02.0	+12 47 30	0.15	-6.1	-2.58 ± 0.47	2	2.72	5.39	2.2	uFd
Draco	17 20 01.4	+57 54 34	0.08	-8.7	-2.00 ± 0.70	1	2.19	6.45	2.9	dSph
Sag dSph	18 55 03.1	-30 28 42	0.02	-12.7	-0.50 ± 0.80	1	1.99	8.02	5.3	dSph
Sag dIrr	19 29 59.0	-17 40 41	1.04	-11.5	-2.30 ± 0.40	1	6.94	6.51	-0.2	dIrr
NGC6822	19 44 57.7	-14 48 11	0.50	-15.2	-1.20 ± 0.40	1	8.15	8.34	0.6	dIrr
Tucana	22 41 49.0	-64 25 12	0.88	-9.2	-1.70 ± 0.20	1	4.18	6.62	0.0	dTran
PiscesII	22 58 31.0	+05 57 09	0.18	-4.4	-	-	-	4.70	1.9	uFd
M31 Group										
WLM	00 01 58.1	-15 27 40	0.97	-14.1	-1.40 ± 0.40	1	7.83	7.69	0.2	dIrr
And XVIII	00 02 14.5	+45 05 20	1.36	-9.1	-	-	-	6.60	0.5	dSph
And XX	00 07 30.7	+35 07 56	0.80	-5.8	-	-	-	5.26	2.4	dSph
And XIX	00 19 32.1	+35 02 37	0.93	-8.3	-	-	-	6.28	1.9	dSph
IC10	00 20 24.5	+59 17 30	0.66	-16.0	-1.30 ± 0.40	1	8.00	8.47	1.6	dIrr
And XXVI	00 23 45.6	+47 54 58	0.76	-6.5	-	-	-	5.54	2.9	dSph
Cetus	00 26 11.0	-11 02 40	0.78	-10.2	-1.70 ± 0.20	1	4.18	7.02	0.5	dTran
And XXV	00 30 08.9	+46 51 07	0.81	-9.1	-	-	-	6.58	2.9	dSph
NGC147	00 33 11.6	+48 30 28	0.76	-14.8	-1.10 ± 0.40	1	3.74	8.21	2.8	dSph
And III	00 35 33.8	+36 29 52	0.75	-9.3	-1.70 ± 0.20	1	5.55	6.66	3.2	dSph
And XXX	00 36 34.9	+49 38 48	0.68	-	-	-	-	-	2.4	-
And XVII	00 37 07.0	+44 19 20	0.74	-7.0	-	-	5.54	5.74	3.6	dSph
And XXVII	00 37 27.1	+45 23 13	0.83	-7.3	-	-	-	5.88	3.1	dSph
NGC185	00 38 58.0	+48 20 10	0.61	-14.7	-0.80 ± 0.40	1	5.02	8.29	2.0	dE
NGC205	00 40 22.5	+41 41 11	0.82	-16.1	-0.50 ± 0.50	1	5.60	8.92	3.6	dE
M32	00 42 42.1	+40 51 59	0.49	-14.8	-1.10 ± 0.60	1	6.00	8.65	1.5	dE
And I	00 45 40.0	+38 02 14	0.73	-10.7	-1.40 ± 0.20	1	5.53	7.21	3.4	dSph
And XI	00 46 20.0	+33 48 05	0.73	-6.2	-1.75 ± 0.18	3	5.53	5.42	2.7	dSph
And XII	00 47 27.0	+34 22 29	0.83	-6.4	-	-	5.64	5.51	2.6	dSph
And XIV	00 51 35.0	+29 41 49	0.73	-7.7	-	-	5.53	6.03	2.2	dSph
And XIII	00 51 51.0	+33 00 16	0.84	-6.8	-1.74 ± 0.18	3	5.65	5.66	2.4	dSph
And IX	00 52 52.8	+43 12 00	0.79	-8.1	-	-	5.60	6.20	4.0	dSph
And XVI	00 59 29.8	+32 22 36	0.52	-8.2	-	-	5.24	6.23	1.6	dSph
LGS 3	01 03 55.0	+21 53 06	0.65	-9.3	-1.70 ± 0.30	1	5.02	5.96	1.5	dTran
IC1613	01 04 47.8	+02 08 00	0.73	-14.5	-1.40 ± 0.30	1	7.77	8.07	0.8	dIrr
And X	01 06 33.7	+44 48 16	0.63	-7.9	-	-	5.40	6.10	2.2	dSph
And V	01 10 17.1	+47 37 41	0.81	-9.2	-1.90 ± 0.10	1	5.62	6.62	2.6	dSph
And XV	01 14 18.7	+38 07 03	0.76	-8.7	-	-	5.56	6.43	2.9	dSph
And II	01 16 29.8	+33 25 09	0.65	-9.2	-1.50 ± 0.30	1	5.44	6.65	2.1	dSph
And XXIV	01 18 30.0	+46 21 58	0.60	-7.0	-	-	-	5.77	1.9	dSph
And XXII	01 27 40.0	+28 05 25	0.79	-6.0	-	-	-	5.36	2.3	dSph
And XXIII	01 29 21.8	+38 43 08	0.73	-9.5	-	-	-	6.75	2.5	dSph
LeoA	09 59 26.4	+30 44 47	0.81	-11.7	-2.10 ± 0.40	1	7.04	6.93	0.1	dIrr
KKR25	16 13 47.6	+54 22 16	1.86	-9.4	-2.10 ± 0.40	1	4.91	6.71	-0.6	dTran
DDO210	20 46 51.8	-12 50 53	0.94	-11.1	-1.90 ± 0.30	1	6.42	6.75	0.0	dTran
IC5152	22 02 41.9	-51 17 43	1.97	-15.6	-1.40 ± 0.50	1	8.02	8.72	-0.7	BCD
And XXVIII	22 32 41.2	+31 12 58	0.65	-7.7	-	-	-	6.04	1.2	dTran
Cas dSph	23 26 31.8	+50 40 32	0.79	-11.7	-1.50 ± 0.20	1	5.60	7.62	1.8	dSph
Pegasus	23 28 34.1	+14 44 48	0.76	-11.5	-2.00 ± 0.30	1	6.53	7.13	1.0	dIrr
Peg dSph	23 51 46.4	+24 35 10	0.82	-10.7	-1.70 ± 0.20	1	4.21	7.22	1.5	dSph

TABLE 5 — *Continued*

Object	RA (J2000)	Dec. (J2000)	D_{\odot}	M_B	$\langle[Fe/H]\rangle$	Ref	$\log M_{HI}$	$\log L_K$	Θ_5	Type
And XXI	23 54 47.7	+42 28 15	0.86	-9.3	-	-	-	6.66	2.2	dSph
And XXIX	23 58 55.6	+30 45 20	0.73	-7.5	-	-	-	5.96	2.0	dSph
Antlia Group										
NGC3109	10 03 07.2	-26 09 36	1.32	-15.7	-1.70 ± 0.40	1	8.37	8.57	0.2	dIrr
Antlia	10 04 04.0	-27 19 55	1.32	-9.8	-1.90 ± 0.20	1	5.92	6.47	2.3	dTran
Sculptor Group										
ESO410-G005	00 15 31.4	-32 10 48	1.82	-11.6	-1.64 ± 0.03	this study	5.91	6.88	0.2	dTran
ESO294-G010	00 26 33.3	-41 51 20	1.88	-10.9	-1.77 ± 0.03	this study	5.48	6.25	0.5	dTran

REFERENCES. — 1. Grebel, E. K., Gallagher, J. S., III, & Harbeck, D. 2003; 2. Norris, J. E. et al. 2010, ApJ, 723, 1632; 3. Yang & Sarajedini 2012 (YS12); 4. Kirby, E. N., Simon, J. D., Geha, M., Guhathakurta, P., & Frebel, A. 2008; 5. Willman, B. et al. 2011